ISSN 0915-633X

NATIONAL INSTITUTE FOR FUSION SCIENCE

The Role of Stochasticity in Sawtooth Oscillation

A. J. Lichtenberg, K. Itoh, S.-I. Itoh
and A. Fukuyama

(Received – July 26, 1991)

NIFS-103 Aug. 1991

RESEARCH REPORT
NIFS Series

NAGOYA, JAPAN

The Role of Stochasticity in Sawtooth Oscillation

Allan J. Lichtenberg

Department of Electrical Engineering and Computer Science

University of California, Berkeley, CA 94720

Kimitaka Itoh and Sanae-I. Itoh

National Institute for Fusion Science, Chikusaku Nagoya 464-01

Atsushi Fukuyama

Faculty of Engineering, Okayama University, Okayama 700

Keywords:
Sawtooth Oscillations, Stochastically Enhanced Transport Coefficients, Magnetic Trigger, Fast Sawtooth Crash, Partial Reconnection

Abstract

Stochastization of field lines, resulting from the interaction of the fundamental m/n=1/1 helical mode with other periodicities, plays an important role in sawtooth oscillations. The time scale for the stochastic temperature diffusion is shown to be sufficiently fast to account for the fast sawtooth crash. The enhanced electron and ion viscosity, arising from the stochastic field lines, are calculated. The enhanced electron viscosity always leads to an initial increase in the growth rate of the mode, the "magnetic trigger". The enhanced ion viscosity can ultimately lead to mode stabilization before a complete temperature redistribution or flux reconnection has occurred. A dynamical model is introduced to calculate the path of the sawtooth oscillation through a parameter space of shear and amplitude of the helical perturbation, including a stochastic trigger to an enhanced growth rate, stabilization by ion viscosity, and a prescription for flux reconnection at the end of the growth phase.

Our model predicts that four types of the sawtooth oscillations are possible even for a plasma with *monotonic* q(r) profile. There are two types of rearrangement of the magnetic configuration: a partial-magnetic reconnection, in which the safety factor on axis q(0) value oscillates around 0.7 with $\delta q(0) \simeq 0.05$; and a full magnetic reconnection, for which q(0) oscillates between 1 and about 0.8. In a partial reconnection the temperature flattening is rapid and can be either limited to an annulus near the

q=1 rational surface , which then gradually propagates to the axis, or the temperature on axis $T_e(0)$ can rapidly decay, when the stochastic region invades the geometrical axis. With a full magnetic reconnection, $T_e(0)$ collapses rapidly when stochasticity is present or slowly without stochasticity. The main features of the model are compared with experimental observations. In particular, they may explain the sudden growth of the helical perturbation, the "magnetic trigger", the fast time scale of the temperature collapse, a partial temperature collapse, and the persistence of an m/n=1/1 island throughout the sawtooth cycle.

§1 Introduction

A tokamak is subject to resistive instabilities on rational surfaces. If the rotational transform $\iota = 1/q = 1$ within the plasma, then the central core is subject to large amplitude relaxation of the central temperature, known as sawtooth oscillations.[1-3] These oscillations play an important role in limiting the core temperature and therefore considerable attention has been given to understanding their mechanism.

The sawtooth oscillations are characterized by a relatively slow build-up of temperature on the axis(msec time scale) followed by a fast temperature crash ($<100\mu$sec) within the $q=1$ radius. Before the crash a temperature flattening around the $q=1$ surface occurs with $m/n=1/1$ helical symmetry (the magnetic island). Depending on the state of the plasma, a decaying helical perturbation can somtimes be seen after the crash.

Both the linear and the nonlinear growth of the instability, [4-7] and the time needed to build up the core temperature after a crash, have been calculated.[8-10] One explanation of the sawtooth is that there is a full collapse of both the current and the temperature, due to a growing magnetic island which reconnects all of the core flux.[11] Experimental results, however, have given rise to serious objections to this picture. A general objection is that the reconnection mechanism is too slow to account for the crash phase[2]. This discrepancy has become more pronounced as machines have increased in size.[12] A second objection is that a complete reconnection is not always observed.

An early soft X-ray tomographic measurement on the TFR tokamak indicated that the m/n=1/1 island did not grow to encompass a large fraction of the central core region and the island also persisted after the crash, implying that the reconnection was not complete.[3] Thirdly, the experiments have observed a sudden acceleration of the growth of the helical deformation, the "magnetic trigger", which remains unexplained.

Complicated dynamics can often be observed, associated with sawteeth. Recently, particularly associated with the large devices JET and TFTR, these phenomena have aroused new interest.[13,14] For example, the m/n=1/1 island can sometimes be seen to decay after the crash, indicating that a complete reconnection has not occurred. This phenomenon is not always seen (but neither is the precurser oscillation) allowing various interpretations. The crash phase in JET has shown slow partial crashes, fast partial crashes and complete crashes. The growth of the island sometimes appears to increase rapidly, just before a fast crash occurs.[13] In TFTR, a similar sawtooth structure, called a "compound sawtooth", was observed.[14] None of these phenomena are easily explained within the simple reconnection picture.

Various explanations have been advanced to explain the fast crash. One explanation is that the mode is ideal, rather than resistive.[15] This could only occur, however, if the q-values within the q=1 surface remain very close to unity.

An alternative picture of the crash can be drawn by using the concept of intrinsic stochasticity driven by the strong inter-

action of "overlapping" island chains with different helicity. [16-21] The interaction of neighboring islands to produce stochasticity leading to major disruptions, has been examined by a number of authors, including numerical studies.[8,18] It has also been pointed out that the current sheet formed at an island separatrix should give rise to turbulent diffusion.[9] This is related to the mechanism for generating stochastic field lines by the interaction of higher-order islands. Such interactions are always present, as stochasticity is known to be a generic property near island separatrices. The appearance of stochasticity was also examined for a general field perturbation applicable to tearing modes.[20,21]

Physically, second-order islands are formed by beating the poloidal variation of the equilibrium m/n=1/0 with the harmonics of the slow variation of the field line as it encircles m/n=1/1 helical island. Since the second-order islands grow exponentially with respect to the main island size, this leads to a stochasticization time(disruptive time) that is short compared to the island formation time.[21] Electron temperature can rapidly diffuse across this stochastic region to flatten the temperature distribution about the q=1 surface. As we shall see, the presence of stochasticity also allows an increase in the growth rate of the mode. The stochasticity arising from the second order island overlap is shear-dependent, which depends on q(0). If q(0) falls much below 1, large-scale stochasticity becomes important, while if $q(0) \simeq 1$, the stochasticity is much less important.

Because alternative mechanisms for the crash are strongly

dependent on the shear and consequently q(0), measurements of this quantity have been very important for distinguishing between the alternatives. Recently, measurements of the time variation of q(0) on TEXTOR have been made by Faraday rotation experiments.[22] The result shows that q(0) remains well below 1, varying between about 0.8 after the crash to about 0.7 just before the next crash. Measurements of q(0) on JET[23] and TEXT[24] give similar results. The value of q(0)≈0.7 is consistent with a strongly stochastic crash phase, lending credence to this explanation.

A temperature crash resulting from stochastization of field lines also leaves open the possibility of partial reconnection, since the temperature flattening is decoupled from the current flattening. Numerical codes, with q considerably below 1 at the time of temperature crash, have indicated that the field lines are stochastic during the final stage of the mode growth.[25,26] However they have also indicated complete reconnection, and have thus not explained the existence of partial reconnections and postcursor oscillations.

In this paper we shall first review, in Sec.2, the basis for the creation of stochastic field lines. The timescale for the stochastic temperature diffusion will be determined and compared to the time scale for the redistribution of current. We shall show that, depending primarily on the shear but also on other machine parameters, the temperature redistribution and the flux reconnection can either be partial or complete. The enhancement of electron and ion viscosity, arising from the stochastic field

lines, will be determined. The enhanced electron viscosity always leads to an initial increase in the growth rate of the mode, increasing the reconnection speed at the X-point. The enhanced ion viscosity may ultimately lead to the mode stabilization before a complete temperature redistribution or flux reconnection has occurred.

In Section 3 a dynamical model is introduced to calculate the path of the sawtooth oscillation through a parameter space of shear and amplitude of the helical perturbation. The model distinguishes between the different cases of temperature flattening and of magnetic field reconnection, such that the each trajectory can be separately explored. The stochastic trigger to the enhanced growth rate and the stabilization by ion viscosity are also included in the model. We also compare the results to experimental observations, showing that many of the interesting phenomena observed in experiments fall within the range of consequences of our model. In particular, the fast crash and the distinction between full and partial temperature collapse as well as the fast magnetic trigger will be related to experiments.

Finally, in Sec.4 we summarize our results and discuss their implications. We relate our work to other models and compare to computer simulations. A prescription for more detailed numerical analysis will be given.

§2 Sawtooth Physics

2-1 The Island Formation and Thickness of Stochastic Layers

We employ a Hamiltonian formalism to describe the behavior of magnetic field lines. In a tokamak configuration shown in Fig.1, the toroidal coordinate ϕ plays the role of time in the usual dynamical system. When the equilibrium magnetic field forms a closed flux surface, the periodic motion of the unperturbed field line is conveniently described in terms of the action-angle variables, J and θ. The action J labels the flux surface and the change of the angle θ of the unperturbed field line is given by

$$\frac{d\theta}{d\phi} = \frac{dH_0(J)}{dJ} = \iota(J). \qquad (2\text{-}1)$$

The action-derivative of the unperturbed Hamiltonian H_0 yields the rotational transform ι. We note that, in the case of a circular cross section, $J = r^2/2$ and $\iota = RB_r/rB_\phi$.

In the presence of a perturbing field, the Hamiltonian of the field line takes the form

$$H(J,\theta,\phi) = H_0(J) + \Sigma A_{mnk}(\sqrt{2J}/R_0)^{|k|} e^{i(m+k)\theta - in\phi} \qquad (2\text{-}2)$$

where the summation over k is the expansion of the toroidal

correction and m and n are the poloidal and toroidal mode number of the perturbation. Since the equations for the magnetic field line have the following form:

$$\frac{dJ}{d\phi} = \frac{\partial H}{\partial \theta}$$

$$\frac{d\theta}{d\phi} = -\frac{\partial H}{\partial J} \qquad (2\text{-}3)$$

the amplitude of the perturbation A_{mnk} is related to the radial magnetic field B_r as

$$A_{mnk} \simeq \frac{rR_0 B_{rmn}}{i(n+k)B_{\phi 0}} \quad . \qquad (2\text{-}4)$$

We shall assume that the primary island amplitude is determined by the lowest order perturbation term m=n=1. We transform to new variables in a rotating coordinate system, $\hat{J}$, $\hat{\theta}$, and expand around the resonant magnetic surface J_0, where $\iota(J_0)=1$:

$$\hat{\theta} = \theta - \phi,$$

$$\Delta J = J - J_0 \quad (\hat{J} = J) \qquad (2\text{-}5)$$

giving the Hamiltonian for the perturbation:

$$H(\hat{J},\hat{\theta},\Phi) \simeq \left.\frac{d\iota}{dJ}\right|_{J=J_0} \cdot \frac{(\Delta J)^2}{2} + A_{11}\cos\hat{\theta}$$

$$+ \Sigma A_{mnk}(r_1/R_0)^{|k|} e^{i(m+k)\hat{\theta} - i(m+k-n)\Phi} \qquad (2\text{-}6)$$

where we have added the ±1 terms (assumed equal to obtain a pendulum in lowest order) and evaluated the perturbation at $J_0 = r_1^2/2$.

Averaging over the fast variable Φ, we obtain the pendulum Hamiltonian characterizing m/n=1/1 island

$$K_0 = G(\Delta J)^2/2 + F\cos\hat{\theta} \qquad (2\text{-}7)$$

where $F = A_{11}$ and $G = -d\iota/dJ$. Substituting for A_{11} from (2-4) and using a parabolic approximation for ι, F and G are written in terms of the fields as

$$F = r_1 R_0 B_r/B_\Phi \equiv r_1^2 \tilde{B}_n \qquad (2\text{-}8)$$

and

$$G = 2(\iota(0)-1)/r_1^2 \equiv 2s/r_1^2 \qquad (2\text{-}9)$$

Here $\tilde{B}_n$ is the normalized perturbation field and $s = \iota(0)-1$ is the normalized shear. The amplitude of the island and the frequency

at the fixed point are given by

$$\Delta J_M = 2(F/G)^{1/2} = (8\tilde{B}_n/s)^{1/2} \qquad (2\text{-}10)$$

and

$$\omega_0 = (FG)^{1/2} = (2\tilde{B}_n s)^{1/2}. \qquad (2\text{-}11)$$

To obtain the thickness of the stochastic layer, we transform to new action-angle variables, I and θ, in the pendulum Hamiltonian frame, to exhibit the second order islands. Retaining the rapidly varying terms, we have a Hamiltonian of the form

$$K(I, \theta, \phi) = K_0(I)$$

$$+ \Sigma A_{mnk}(r_1/R_0)^{|k|}\Sigma V_\ell e^{i\ell\theta + i(m-k-n)\phi} \qquad (2\text{-}12)$$

where V_ℓ are the coefficients of the Fourier expansion of $e^{i(k+m)\hat{\theta}}$ with respect to θ. Harmonic terms resonate with the nonlinear motion of frequency $\omega(I) = dK_0/dI$, if $\ell\omega+m+k-n=0$ is satisfied and the second-order islands are formed on the resonant action surfaces. The thickness of the stochastic layer around the main island separatrix can be estimated by the overlap condition of the second-order islands. Since $\omega(I)<<1$ when the stochastic layer first appears, we only consider the harmonic terms

with $m+k-n = \pm 1$. Since $r/R_0 \ll 1$, we look at small k. For harmonics with q =1 helical symmetry, m=n=1 for which $k = \pm 1$.

Considering this mode only, we can derive the overlap condition for two second-order islands chains[21]. In the spirit of our approximate calculation, we use a simple form obtained from the separatrix mapping approximation[27]. The result is

$$\delta J_S = 2\left(\frac{F}{G}\right)^{1/2} \frac{4\pi}{(FG)^{3/2}} \exp\left(-\frac{\pi}{2(FG)^{1/2}}\right) \qquad (2\text{-}13)$$

where δJ_S is the half-thickness of the separatrix layer which is approximately equal inside and outside of the separatrix. The edge of the regular region, outside and inside of the separatrix are then calculated from

$$\Delta J_T = \Delta J_M \pm \delta J_S \qquad (2\text{-}14)$$

with the + and - signs indicating the outside and inside edges, respectively. This result can also be easily transformed to physical space, using

$$r = r_1(1 - \Delta J_T/J_0)^{1/2} \qquad (2\text{-}15)$$

and $\Delta r_T = r - r_1$. The result in (2-15) is plotted in Fig.2(a). We see that a thick stochastic layer forms when $\ell(0) = (FG)^{-1/2} = 6$. A more accurate calculation of the second-order islands, includ-

ing the full elliptic integral representations of the harmonic amplitudes was done and compared to a numerical calculation with the same assumed harmonic field[21]. The result indicated that a significant layer of stochasticity already appears at the island edge for

$$\ell(0) = (FG)^{-1/2} \simeq 7. \qquad (2\text{-}16)$$

We also see from Fig.2(a) that the center of the island is not stochastic even when the stochasticity has reached the axis.

We note that the thickness of the stochastic layer near the X-point is greatly enhanced. Using the form in (2-7) for an initial condition outside the separatrix at the edge of the stochastic layer, taken at $\Delta J_M + \delta J_S$ where δJ_S is the thickness of the stochastic layer as a obtained from (2-13), the thickness of the stochastic layer near the X-point is calculated from

$$G\delta J_x^2/2 + F = G(\Delta J_M+\delta J_S)^2/2 - F \qquad (2\text{-}17)$$

giving to first order

$$\delta J_x \simeq (\Delta J_M \delta J_S)^{1/2} \qquad (2\text{-}18)$$

which is the geometric mean between a (relatively) thin separatrix layer and the large amplitude of the primary island.

Finally, we derive the condition for which a sizeable stochastic layer appears before the primary island touches the

magnetic axis. From(2-19), the condition $\Delta J_M \geqq J_0$ can be expressed as

$$4F/G \leqq J_0^2. \tag{2-19}$$

Combining (2-19) and (2-16), we obtain a condition for a thick stochastic layer to form before the island fills the core

$$GJ_0 \ell(0)/2 \geqq 1, \quad \ell(0) \simeq 7. \tag{2-20}$$

In the case of a parabolic rotational-transform profile with $r_1 = a/2$, this condition can be rewritten as [21]

$$q(0)/(1-q(0)) \leqq \ell(0)/2 \tag{2-21}$$

Taking $\ell(0)=7$, the condition (2-21) yields $q(0) \leqq 0.8$. The significance of this result is that for $q(0) < 0.8$ we would expect a temperature crash to occur before a full flux reconnection has occurred. It does not however, tell whether or not the end state is fully reconnected, which depends on self-consistent conditions. We discuss these conditions in the following subsections.

2-2 Stochasticity Enhanced Transport Coefficients and Associated Time scales

In this subsection, we explore various enhanced transport coefficients in the presence of stochasticity. The equations of Visco-resistive MHD are the following:

$$\frac{\partial \mathbf{u}}{\partial t} + \mathbf{u}\cdot\nabla\mathbf{u} = \mathbf{J}\times\mathbf{B} - \nabla p + \underline{\mu_i \nabla^2 \mathbf{u}}, \tag{2-22}$$

$$\frac{\partial \mathbf{A}}{\partial t} = \mathbf{u}\times\mathbf{B} - \eta\mathbf{J} - \underline{\nabla\times\lambda\nabla\times\mathbf{J}}, \tag{2-23}$$

$$\frac{\partial p}{\partial t} + \mathbf{u}\cdot\nabla p = -\Gamma p\nabla\cdot\mathbf{u} + (\kappa_{/\!/}/B^2)(\mathbf{B}\cdot\nabla)^2 p + \underline{\nabla\cdot(\kappa_\perp \nabla p)} + (\Gamma-1)\eta J^2, \tag{2-24}$$

$$\mathbf{B} = \nabla\times\mathbf{A} \text{ and } \mathbf{J} = \nabla\times\mathbf{B}. \tag{2-25}$$

In this section J is the current density, not the action. Equation (2-22) is the force equation, (2-23) is Ohm's law, (2-24) gives energy transport and (2-25) is the low frequency part of Maxwell's equations. Here, μ_i is the ion viscosity, η is the

resistivity λ is the electron viscosity (current viscosity), Γ is the ratio of specific heats, and $\kappa_{\parallel}$ and $\kappa_{\perp}$ are the parallel and perpendicular thermal conductivities, respectively. Normally these equations are solved numerically (or in some small signal analytic approximation) using the classical transport coefficients arising from binary collisions [5-8, 10, 25, 26]. When this is done, the ion viscosity μ_i is unimportant, except for numerical stability, the electron viscosity λ is unimportant compared to the resistivity η, and the transverse heat conductivitiy $\kappa_{\perp}$ only serves to establish the equilibrium pressure distribution on a slow time scale. Once stochasticity appears on a large scale, however, the terms underlined can be greatly enhanced.[28, 29] This can lead to much faster relaxations than are classically obtained.

Let us consider the transport quantities in the presence of stochasticity, and the associated time scales on which processes can occur. The coefficients, $\kappa_{\perp}$ λ and μ_i are derived in Appendix 1, and are examined here, along with the associated time scales for heat transport, current diffusion, reconnection, and the m/n=1/1 visco-resistive MHD mode growth.

$\kappa_{\perp}$: The fastest time scale is for heat to diffuse, which is given directly in terms of the time for electrons to diffuse along with the field lines, giving (from Appendix 1)

$$\kappa_{\perp} = (3/\sqrt{\pi}) n v_{Te} D_M \qquad (2\text{-}26)$$

where v_{Te} is the electron thermal velocity and, for fully developed stochasticity,

$$D_M = (\delta r)^2/2\pi R, \tag{2-27}$$

the quasilinear magnetic field line diffusion in which the field lines step a random distance δr in going once around the torus. The density n is a dimensional scale factor for (2-24). The time for diffusing across a distance Δr is then

$$\tau_\kappa = (\Delta r)^2/D_M v_{Te} = (\Delta r/\delta r)^2 \tau_{tr} \tag{2-28}$$

where $\tau_{tr}=2\pi R/v_{Te}$. The time, given in (2-28) is very fast, as it is related to an electron transit time τ_{tr} by a factor that is in the range of 20-50. For the plasma parameters of JET (R =3m, T_e =5 keV) we have $\tau_{tr} \simeq 0.6$ μsec and $\tau_\kappa \simeq$ 10-25 μsec, readily accounting for $\tau_{crash} \leqq 100\mu$sec.

λ : Stochastic flux lines and rapid heat loss does not imply rapid diffusion of the current. The inductance of the current channel prevents a rapid macroscopic rearrangement of the flux. The long-time scale on which this occurs can also be calculated. From Appendix 1 we have the electron viscosity

$$\lambda = \frac{\sqrt{\pi}}{2}\mu_0 \frac{c^2}{\omega_p^2} v_{Te} D_M . \tag{2-29}$$

We find a new factor of the square of the collisionless skin depth $\delta_s = c/\omega_p$ multiplying the coefficient in a term in (2-23) which is fourth derivative of the spatial variation. The result is a time scale for current flattening over radial extent Δr,

$$\tau_\lambda = (\Delta r/\delta_s)^2(\Delta r/\delta r)^2\tau_{tr} \qquad (2\text{-}30)$$

$$= (\Delta r/\delta_s)^2\tau_\kappa.$$

The collisionless skin depth is of the order of 10^{-4}m for the higher density tokamaks ($10^{19}\text{m}^{-3} \leqq n_e \leqq 10^{20}\text{m}^{-3}$). For JET parameters with $\Delta r \sim 0.1$m, we find $\tau_\lambda = 100\text{-}200$msec. From experimental data, we see that this time scale is too long for any significant current flattening during the crash. It can, however, be an important mechanism on the sawtooth time scale, since only a small reordering of current is required to return the current distribution to an initial state.

There is, however, a faster time scale on which the currents can be rearranged, which is by magnetic flux reconnection. Based on the Sweet-Parker reconnection model, Kadomtsev[11] has estimated the reconnection speed by requiring the flow of the bulk reconnecting flux to just balance the Alfven flow into the δ_{rec} separatrix current channel, i.e.,

$$r_1/\tau_{rec} = \delta_{rec}/\tau_{Ah} \qquad (2\text{-}31)$$

where r_1 is the radius of the q=1 surface(X-point) and τ_{rec} is the reconnection time, r_1/v_r. Here

$$\tau_{Ah} = r_1/v_{Ah},$$

$$v_{Ah} = B^*/\sqrt{\mu_0 m_i n_i}$$

where v_{Ah} is the Alfven velocity associated with the helical magnetic field, $B^*=(1-q(r))B_\theta$ and μ_0 is the free space permitivity. The reconnection speed limits the large amplitude growth of helical deformation of the magnetic axis ξ such that,

$$\tau\xi < \delta_{rec}/\tau_{Ah}$$

where ξ is the deformation of the magnetic axis.

We can extend this argument keeping the electron viscosity term λ in the estimation of δ_{rec}. The parallel component of Ohm's law is rewritten as

$$E + v_r B^* = \eta J - \lambda \nabla^2 J \qquad (2\text{-}32)$$

Estimating $J=B^*/(\mu_0\delta_{rec})$ and $\nabla^2 J \simeq -J/\delta_{rec}^2$ with the approximation of $E \sim v_r B^*$, we obtain the scaling for the rearrangement of the helical flux B^*

$$\frac{\delta_{rec} B^*}{\tau_{Ah}} \simeq \frac{\eta B^*}{\mu_0 \delta_{rec}} + \frac{\lambda B^*}{\mu_0 \delta_{rec}^3}. \qquad (2\text{-}33)$$

Eliminating B^* from (2-33) we find that the reconnection layer scales as

$$\delta_{rec}{}^2 \simeq [(\eta\tau_{Ah}/\mu_0)+\sqrt{(\eta\tau_{Ah}/\mu_0)^2+\lambda\tau_{Ah}/\mu_0}]/2 \qquad (2\text{-}34)$$

The associated reconnection time τ_{rec} is then given from (2-31) by

$$\tau_{rec} \simeq \sqrt{2}\tau_{Ah} r_1 [(\eta\tau_{Ah}/\mu_0)+\sqrt{(\eta\tau_{Ah}/\mu_0)^2+\lambda\tau_{Ah}/\mu_0}]^{-1/2} \qquad (2\text{-}35)$$

In the absence of stochasticity, when λ is small, the reconnection width scales as

$$\delta_{rec} \simeq (\eta\tau_{Ah}/\mu_0)^{1/2}. \qquad (2\text{-}36)$$

In the case in which the mode is sufficiently large that the current layer is covered with stochastic filed lines, then the term in λ dominates over the one in η and is estimated as

$$\delta_{rec} \simeq r_1 \left(\frac{\lambda}{\mu_0 r_1{}^4}\ \frac{r_1}{v_{Ah}}\right)^{1/4}. \qquad (2\text{-}37)$$

Substituting (2-37) in (2-31) the reconnection time due to electron viscosity is then

$$\tau_{rec} \simeq (r_1/\delta_s)^{1/2}(\tau_\kappa \tau_{Ah}^3)^{1/4},$$

where we have substituted for τ_κ from (2-30). Since the λ dependence is weak, $\lambda^{1/4}$, the rapid growth of the magnetic axis deformation is possible even when the mode growth is limited by the reconnection speed, as also described in [30]. For JET parameters a reconnection time scale $\tau_{rec} \simeq 20\text{-}30\mu$sec is found, which is a quite similar value to the energy diffusion (τ_{crash}) time. Although this is a lower bound on the time scale for an actual reconnection, since we expect the current layer to become non-uniform when $\delta_{rec} > \delta_s$, it indicates that stochasticity can be a dominant mechanism in the reconnection process.

μ_i : For a fast reconnection to occur after stochasticity has set in, it is necessary that the mode continue to grow. A stabilizing force on the mode growth is the ion viscosity, which is also strongly enhanced due to the stochasticity. In Appendix 1, we calculate μ_i to be

$$\mu_i = (v_{Ti}/\sqrt{\pi})D_M \qquad (2\text{-}38)$$

such that we can define a relaxation time under the action of ion viscosity given by

$$\tau_{\mu i} = (\Delta r/\delta r)^2(3v_{Te}/v_{Ti})\tau_{tr} . \qquad (2\text{-}39)$$

We can compare the contribution from the ion viscosity, which tends to damp the mode, with the contribution from the electron viscosity which enhances the mode growth. To do this we perform a linearized analysis of the mode growth, using the stochasticity enhanced transport coefficients. The result for the mode growth rate is derived in Appendix 2 and given in (A2-11). Using (2-29) and (2-30) to relate λ to τ_λ and (2-38) and (2-39) to relate μ_i to $\tau_{\mu i}$, (A2-11) can be rewritten in the form

$$\tau\tau_A = 5(2\varepsilon s)^{4/5}\left(\frac{\tau_A}{\tau_\lambda}\right)^{1/5} - 5^{-1/3}(2\varepsilon s)^{2/5}\left(\frac{\tau_A}{\tau_\lambda}\right)^{3/5}\left(\frac{\tau_A}{\tau_{\mu i}}\right) \quad (2\text{-}40)$$

where s is the normalized shear parameter $\iota(0)-1$ and $\varepsilon=r_1/R$. Noting the power of λ (i.e. τ_A/τ_λ) in the first and second terms on the right hand side, we see that , when the stochasticity switches on and λ is small, the first term dominates over the second term and accelerates the mode growth. If the stochastic transport coefficient D_M becomes larger, however, the second term can exceed the first one thus stabilizing the mode. This stabilization can occur before the flux reconnection is complete.

2-3 Parameter Space of Mode Dynamics

To make these competing effects on the mode growth and decay

more transparent, we construct the following diagram in the $\tilde{B}_n$ and s parameter space, where $\tilde{B}_n$ is the normalized perturbation strength. From the viewpoint of magnetic topology, using the equation in (2-19), we have the condition that the island separatrix touches the axis

$$8\tilde{B}_n/s = 1. \qquad (2\text{-}41)$$

If we include the thickness of the stochastic layer outside of the island from (2-13), we obtain the condition for the outermost stochastic field line to touch the axis, that is $|\Delta r_T| = r_I$:

$$(8\tilde{B}_n/s)^{1/2}\left[\, 1 + \frac{4\pi}{(2\tilde{B}_n s)^{3/2}} \exp\left(-\frac{\pi}{2(2\tilde{B}_n s)^{1/2}}\right)\right] = 1 \,. \qquad (2\text{-}42)$$

In Fig.3., lines of (2-41) and (2-42) are plotted as solid lines denoted by (1) and (2), respectively. The region of the parameter space between them corresponds to values for which the stochasticity has reached the axis but the island separatrix has not. Schematic drawings of the magnetic field perturbation are shown in Fig.4. When the perturbation grows until line (2) is reached, the central temperature crash (T-crash) is expected with a time scale of τ_K. If the perturbation grows further until the line (1) is reached, that indicates the completion of the magnetic reconnection. On the same diagram, we draw the dashed

line for $\omega(0) = \sqrt{2\tilde{B}_n s} = 1/12$ (denoted by (3) for which the stochastic layer at the separatrix calculated from (2-18) is equal to the resistive current layer calculated from (2-36). When the perturbation becomes large enough to cross line (3), the mode is accelerated due to the stochasticity enhanced reconnection rate. The upper dashed line, denoted by (4), is that for which the mode becomes stable due to the stochasticity enhanced viscosity, $\tau\tau_A = 0$ in (2-40).

Depending on the position of this upper dashed line (4) with respect to the lower solid line (2), two distinct types of behavior can be observed. Consider the case shown in Fig.3 for which the dashed curve (4) lies mainly above the solid curve (2). Then, provided the shear is sufficiently large that the two solid curves (1) and (2) are well separated, one would expect a complete temperature crash before reaching the stability boundary of the saturated state (4). Depending on where (4) lies with respect to (1), the magnetic reconnection may be either incomplete, when (4) is well below (1) or complete, when (4) lies close to (1).

In the opposite case, in which curve (4) lies below curve (2), the mode would expect to saturate before the stochastic region reached the axis, and neither the temperature crash nor the reconnection would be complete. The stability boundary condition (2-37) shifts upward in Fig.3 for smaller machine size R, for lower density and weakly for higher electron temperature.

If the shear is small, then the path of the growing instability can take the island width to the axis (curve (1)),

without crossing the lowest dashed line(3), such that the stochasticity is negligible. In this case, one might expect a slow complete reconnection.

2-4 Rearrangement of the Magnetic Flux Surface

The process of rearrangement of magnetic flux surface is not fully analyzed in this paper. A crude estimation of the shear after the rearrangement of magnetic field can be done for the following limiting cases.

1) The helical flux in the hot helix is assumed to be unchanged, which is set equal to that within the q=1 surface of a new state. The helical flux in the hot part is estimated by the difference in the fluxes between the value at the X-point and that at the magnetic axis,

$$\Phi_h(r,\theta-\phi)-\Phi_h(\text{axis}) = \frac{1}{r_1^2}\int_o^r r dr[\iota(r) - 1] + 2\tilde{B}_n(\frac{r}{r_1})\cos(\theta-\phi) \quad (2\text{-}43)$$

which on integration for $\theta-\phi = \pi$ (the X-point) gives

$$\Phi_h(\text{X-point}) - \Phi_h(\text{axis}) \simeq [\iota(0)_{old}-1]/4 - 2\tilde{B}_n. \quad (2\text{-}44)$$

The renewed q=1 surface of radius r_1 contains the flux,

$$\Phi_h = [\iota(0)_{new} - 1]/4. \qquad (2\text{-}45)$$

Equating (2-44) and (2-45) we obtain,

$$\iota(0)_{new} = \iota(0)_{old} - 8\tilde{B}_n. \qquad (2\text{-}46)$$

This probably gives an underestimate of $\iota(0)_{new}$ since the cold helical flux may contribute to the central helical flux of the new state, i.e., there is a reverse reconnection through the stochastic layer as the core relaxes back toward the axis.

2) The local pitch ratio near the magnetic axis is assumed to be unchanged when the shift of magnetic axis is reset. Due to the perturbation $\tilde{B}_n$, the magnetic axis of the hot core shifts by an amount

$$\xi = [2\tilde{B}_n/(\iota(0)_{old} - 1)]r_1. \qquad (2\text{-}47)$$

The new rotational transform around the magnetic axis,

$$\partial^2\Phi_h/\partial x^2 = 2[\iota(0)_{new} - 1] \qquad (2\text{-}48a)$$

where the normalized distance between the geometrical axis and the magnetic axis is $x=\xi/r_1$, giving

$$\partial^2\Phi_h/\partial x^2 = 2[1 - 3(\xi/r_1)^2][\iota(0)_{old} - 1]. \qquad (2\text{-}48b)$$

When the curvature is kept unchanged we equate (2-48a) and (2-48b) to obtain

$$\iota(0)_{new}-1 = [1-3(\xi/r_1)^2][\iota(0)_{old}-1]. \qquad (2\text{-}49)$$

In the cases of incomplete reconnection a finite size island remains on the q=1 surface, with an initial flattening of the q in the neighborhood of that surface. Because we believe the reverse reconnection process to be important we use (2-49) to reset $\iota(0)$ in our dynamical calculation.

For the cases in which there is a complete reconnection, the rearrangement of the magnetic flux surface leads to q on the axis being close to unity with a weak shear in the new symmetric equilibrium,[31]

$$\iota(0)_{new} - 1 = \varepsilon^2 . \qquad (2\text{-}50)$$

In this case the island would grow from a quite small value.

§3 The Dynamical Model and Example

3-1 Dynamical Model

Based on the physics modelling in section 2, we develop a dynamical model of the sawtooth oscillations. We choose two variables, the amplitude of the m/n=1/1 mode magnetic perturbation and the magnetic shear at the rational surface. We express the stochasticity as a function of these two variables and follow the temporal evolution. The dynamical equations are that for the growth of the helical magnetic perturbation and that for the change of magnetic shear.

Helical Magnetic Perturbation

The m/n=1/1 component of the magnetic perturbation grows with the growth rate τ as

$$d\tilde{B}_n/dt = \tau\tilde{B}_n, \tag{3-1}$$

where we use two forms for the mode growth rate. If the stochastic layer thickness at the X-point is thinner than that of the current layer at the X-point, we take

$$\tau = \tau_{r0}s^{2/3} \tag{3-2}$$

which is the conventional growth rate of the resistive kink mode, $\tau_{r0} \simeq S^{-1/3}/\tau_{Ap}$, where $S = \tau_r/\tau_{Ap}$ and $\tau_r = \mu_0 r_1^2/\eta$[4]. If

the stochastic layer thickness at the x-point is wider than that of the current layer at x-point, the growth rate is given by the stochastically enhanced growth rate

$$\tau = \tau_s . \tag{3-3}$$

We use the expression for the growth rate τ_s in the presence of the stochastic current viscosity and ion viscosity from (A2-11), which we repeat here

$$\tau_s\left(\frac{R}{v_A}\right) = 5(2\varepsilon s)^{4/5}\left[\frac{\lambda}{\mu_0 r_I^4}\frac{R}{v_A}\right]^{1/5} - 5^{-1/3}(2\varepsilon s)^{2/5}\cdot\alpha\left[\frac{\lambda}{\mu_0 r_I^4}\frac{R}{v_A}\right]^{3/5} \tag{3-4}$$

where

$$\alpha = \frac{2v_{Ti}}{\pi v_{Te}}\left(\frac{\omega_p^2}{c^2} r_I^2\right) \tag{3-5}$$

is the key scaling factor between the electron and ion terms. We can include the transition from weak to fully developed stochasticity by writing λ in the form

$$\frac{\lambda}{\mu_0 r_I^4}\frac{R}{v_A} = \Gamma_0 \tilde{B}_n^2 (D_M / D_{QL}) \tag{3-6}$$

where

$$\Gamma_0 = \left[\frac{c^2}{\omega_p^2 r_1^2}\right] \frac{\pi^{3/2} v_{Te}}{v_A} \tag{3-7}$$

and D_M/D_{QL} is the ratio of the magnetic diffusivity normalized to its quasilinear estimation. By using this notation and the ratio between μ_i and λ (Eqs.(A1-10,11)), the linear growth rate τ_s, for the case of stochastic magnetic field, is expressed as

$$\tau_s\left(\frac{R}{v_A}\right) = 5(2\varepsilon s)^{4/5}\Gamma_0^{1/5}\tilde{B}_n^{2/5}\left[\frac{D_M}{D_{QL}}\right]^{1/5}$$

$$- 5^{-1/3}\alpha(2\varepsilon s)^{2/5}\Gamma_0^{3/5}\tilde{B}_n^{6/5}\left[\frac{D_M}{D_{QL}}\right]^{3/5} \tag{3-8}$$

A simplified model for the magnetic diffusion coefficient is employed, following the standard mapping form [27]

$$D_M/D_{QL} = \min[(\tilde{B}_n/B_c - 1)^3,\ 1]. \tag{3-9}$$

The denominator B_c is the critical amplitude for the onset of stochasticity. We choose this critical value by the rule that the thickness of the stochastic layer at the X-point is equal to

that of the current layer,

$$\delta_x[B_c, s] = \delta_r \tag{3-10}$$

where δ_r is the current layer thickness associated with the resistive mode growth. Equation (3-10) determines B_c as a function of s and δ_r/r_1. As discussed in Sec.2, the condition

$$\ell \simeq 12 \tag{3-11}$$

is an approximate relation to calculate B_c, where $1/\ell$ is the rotational transform around the O-point of the magnetic island. At the onset of stochasticity, the current layer thickness is obtained from Eq.(2-36)

$$\delta_r/r_1 = (\eta\tau_{Ah}/\mu_0 r_1^2)^{1/2} \tag{3-12}$$

This value is of the order of 10^{-2}, and using Eqs.(2-13), (2-18) and (3-10), we obtain an approximate numerical relation

$$B_c \simeq 0.03/s. \tag{3-13}$$

As is seen from Eqs.(2-13) and (2-18), the layer thickness δ_x has an exponential dependence on $1/\sqrt{\tilde{B}_n s}$, so that the dependence of B_c on δ_r/r_1 is only logarithmic. The dependence of the constant 0.03 on the plasma parameters is neglected for simplicity.

Change of Shear

The change of the shear, during most of the growth phase of the magnetic perturbation, is determined by the current peaking resulting from the higher conductivity at the axis. This resistive process has been discussed in the literature [8-10]. When one takes into account the radial inhomogeneity of resistivity due to the neoclassical effect, the dominant term in the q-profile change is given as [10]

$$q(0;t) = 1 - 2\sqrt{\varepsilon}(t/\tau_r)^{1/4} \tag{3-14}$$

where the time t is measured from the time of a complete reconnection. This equation can be rewritten as

$$ds/dt = (4\varepsilon^2)/(\tau_r s^3) \tag{3-15}$$

by using the parabolic approximation for the ι-profile, which can be integrated for an arbitrary initial value of s.

When stochasticity is present, the current diffusivity λ becomes the dominant mechanism for changing the shear parameter. Combining Ampere's law $\partial B/\partial t = -\nabla\times E$ with the Ohm's law with current diffusion, $E_z = -\lambda\nabla^2 J_z$, we have an equation for the quantity $\Phi = B_\theta/r$ as

$$\partial\Phi/\partial t = -(\lambda/\mu_0)\nabla^4(r\Phi) \tag{3-16}$$

Taylor-expanding Φ in the vicinity of $r=r_1$ as

$$\Phi = \Phi_0 + (r-r_1)\Phi' + \cdots\cdots\cdots \qquad (3\text{-}17)$$

we have

$$\partial\Phi/\partial t = 3\lambda r^{-3}[\ \Phi'_1 + (r_1{}^2/2)\Phi'''_1 + \cdots\cdot] \qquad (3\text{-}18)$$

where the suffix 1 indicates the value at $r=r_1$. This relation gives

$$\partial\Phi'_1/\partial t = -9\lambda/(\mu_0 r_1^4)[\Phi_1' + (r_1^2/2)\Phi_1''' \cdots\ ]. \qquad (3\text{-}19)$$

From the relation $s=(r_1/2)(d\iota/dr)$ and the parabolic approximation of ι with constant B_t, we have

$$\partial s/\partial t - (\dot{r}_1/r_1)s = -9(\lambda r_1{}^{-4})s\ . \qquad (3\text{-}20)$$

Summing up the resistive contribution (3-15) and that by the current diffusivity (3-20), we have

$$ds/dt = \rho/s^3 - \tau_n s, \qquad (3\text{-}21)$$

where

$$\rho = 4\varepsilon^2/\tau_r \qquad (3\text{-}22a)$$

and

$$\tau_n = 9\lambda/(\mu_0 r_1^4) - \dot{r}_1/r_1 \ . \qquad (3\text{-}22b)$$

We assume $\dot{r}_1/r_1$ is small and neglect it for the calculation.

During the sawtooth ramp, but before there is significant stochasticity, only the ρ/s^3 term is present, increasing the shear. After the onset of stochasticity, the term $-\tau_n s$ is dominant, but the time-scale for decreasing the shear is long compared to the mode growth time. After the mode is stabilized by ion viscosity, this term becomes important for decreasing the shear. Because the return path through the parameter space is not precisely known, we use the alternative picture for resetting the shear, as described in Sec. 2.

Post Crash: Partial Magnetic Reconnection

If the mode growth stops at finite amplitude without full magnetic reconnection, the helical structure remains for a much longer time than the stochastically enhanced growth time. Although it is difficult to quantify the mode evolution after a partial reconnection, we can qualitatively identify three stages after the temperature crash and mode stabilization. In the first phase, the stochastic diffusion tends to poloidally symmetrize the helical current in the stochastic portion of the island. This corresponds to the postcursor decay. In the second phase, the mode begins to grow from a finite amplitude island but with a locally flattened q-profile around the q=1 surface. In the third phase, the mode grows with the classical reconnection time const-

ant (if the amplitude is large enough to be in the classical reconnection phase, if not with the linear growth rate) until the condition for stochastic mode acceleration is again established. Estimating the decay time for the first phase

$$\tau_{decay} = \mu_0 \Delta r_x^4 / \lambda \qquad (3\text{-}23)$$

where Δr_x is the thickness of the diffused layer around the rational surface, we have $\tau_{decay} \simeq 23$ms for the parameters of JET (Δr_x= 5cm, $c/\omega_{pe} \simeq 0.08$cm and $\lambda = 1.7 \times 10^{-10}$). This is comparable to the decay time of the postcursor as observed in JET. For the second phase, we take $\tau_r r_1 / v_{Ap} = 10^{-4}$, from Ref.[32], which gives 4 ms for one e-folding growth ($v_A = 8 \times 10^6$m/s, R=3m). For a partial reconnection we assume that the initial perturbation to start the sawtooth is $B_{ni} = 10^{-3}$ (island size is about one tenth of r_1). This value is consistent with observations that a helical structure can remain during the entire sawtooth period as is clearly seen in the phenomenon of the "snake"[33]. In this case, 10ms is necessary to reach $\tilde{B}_n = .01$, which is characteristic threshold value for the stochasticity. The Sweet-Parker reconnection time is about 3ms which is approximately equal to one e-folding time at the reduced growth rate. Summing up these time constants, the total time of these three processes would be about the 40ms observed experimentally. About half of the time is mode decay and about half mode growth, allowing only a few e-foldings from an initial significant amplitude island. For our simplified model we adjust the growth rate τ_r to achieve an appropriate

match to the ramp time, and explore the effect on the dynamics of variations in the growth time. We do not directly follow the decay process of this helical structure during the first phase but include this period in our adjusted growth rate.

As the model for the shear of new symmetric state after the partial magnetic collapse, we choose the second model in §2.4 for the first step of the analysis. Assuming a parabolic current distribution, the shear is obtained from Eq.(2-49) as

$$s(new) = [1 - 3(2\tilde{B}_n/s)^2]s \qquad (3\text{-}24)$$

if the mode stabilization occurs before the magnetic axis and X-point merge. In addition to setting the shear parameter to the new value we choose a reduced amplitude for the m/n=1/1 magnetic perturbation $\tilde{B}_n=B_{ni}$, as described above. We follow the development of ($\tilde{B}_n$, s) using these initial values.

Post Crash: Full Magnetic Reconnection

If the mode growth continues until the magnetic axis and the x-point merge, then we assume that the full reconnection of the Kadomtsev model occurs, with

$$s(new) = \varepsilon^2. \qquad (3\text{-}25)$$

In this case, the remaining amplitude of the helical perturbation would be very small as was shown in many numerical simulations [25,26]. We choose B_{ni} of the order of $10^{-5\sim6}$ in this situation,

which is adjusted to give a reasonable oscillation of q(0), with the mode growth rate taken to be the combination of the linear and reconnection values.

3.2 Examples of dynamical oscillations

We show typical examples of the temporal evolution following the model equations (3-1) and (3-21) with the conditions (3-24), [or (3-25)] and the appropriate B_{ni}. We find four types of sawtooth oscillations, depending on the parameters. The four types are tabulated in Table 1. Types [I] to [IV] are as follows.

[I] The first type is characterized by rapid growth after stochasticity sets in followed by the stabilization of the magnetic perturbation before the stochasticity reaches the magnetic axis. The temperature crash is not complete and an m/n=1/1 island persists.

[II] The second type is associated with the propagation of the stochastic layer to the axis, but the mode is stabilized before the full magnetic reconnection occurs. The central temperature is flattened, but a m/n=1/1 island persists.

[III] The third type includes a full magnetic reconnection. Stochasticity develops before the complete magnetic reconnection occurs, leading to an enhanced growth rate.

[IV] The fourth type is free from stochasticity and includes

the complete magnetic reconnection. In type [IV], the mode growth is slow during the entire reconnection such that an experimental distinction can be made from case [III].

Figure 5 is an example of case [I]. We choose the typical parameters of a JET Ohmic plasma[34]; R = 3m, B_t = 3.45T, $T_e(0)$ = 4keV, $T_i(0)$ = 3keV, $n_e(0) = 6.5\times10^{19}/m^3$, deuterium ions, and ε = 0.1. These parameters correspond to α = 1800, $\Gamma_0 = 7\times10^{-5}$, and $\tau_r v_A/R \sim 10^7$. We choose the normalized linear growth rate in the non-stochastic region as $\tau_{r0} = 10^{-5}/\tau_A$. A reduced growth rate has been used to account for the reduction of the linear growth rate due to the local flattening of the q-profile, and the delay in the growth due to the decay phase after the collapse. We also take $B_{ni} = 10^{-3}$, noting the fact that the island width of the order of $0.1r_1$ seems persistent during the whole sawtooth period with a partial magnetic collapse.

The development of the shear and magnetic perturbation is shown. The q value on axis oscillates around 0.7. The initial value solution of $(\tilde{B}_n, s)$ merges to a periodic oscillation. An expanded time scale is also shown at the onset of the rapid growth in (c). The growth rate changes substantially on a time scale less than $100\tau_A$. Figure 5(d) also illustrates the development of the stochastic region in the radial direction at the onset of the rapid magnetic growth. The mode saturates before the stochastic layer touches the geometrical axis. The typical value of the change of the shear parameter (or equivalently, $\iota(0)$) by the magnetic rearrangement is of the order of 0.05. The

decay phase of the perturbation is not modeled in time; the successive calculations are made by the initialization rule of (3-24). This holds for Figs.6 to 8 also.

The second example in Fig.6 is for case [II]. We choose a slightly lower density, $n_e(0) = 4\times10^{19}/m^3$. Other parameters are the same as in Fig.5. The periodic change of s and B_n is shown. The dynamics is also characterized by a sudden change of the growth rate of the mode, and by a fractional reduction of shear after the crash. The expanded time scale near the stochastic trigger is also shown in (c) and (d). The stochasticity region reaches the geometric center before the mode amplitude stops growing. In this case the full collapse of electron temperature would be observed. A similar value for the change of $\iota(0)$ at the crash is obtained compared to the first case ($\sim$0.07 in this case).

The change from type [I] to type [II] by decreasing the density is understood by studying the marginal stability condition, $\tau_s \simeq 0$. This can be written, in the quasilinear limit, $D_M/D_{QL}=1$, as

$$0.117(2\varepsilon s)^{-2/5}\left(\frac{2v_{Ti}}{\pi v_{Te}}\right)\left(\frac{c}{\omega_p r_1}\right)^{-6/5}\left(\frac{\pi^{3/2}v_{Te}}{v_A}\right)^{2/5}\tilde{B}_n^{4/5} = 1 \quad (3\text{-}26)$$

Expressing R, n_e, T_e, B_t in m, $10^{20}/m^3$, keV and Tesla, respectively, we have

$$\tilde{B}_n^{4/5} = 0.033 s^{2/5} \varepsilon^{-4/5} R_m^{-6/5} n_{20}^{-4/5} T_{keV}^{-1/5} B_T^{2/5} \qquad (3\text{-}27)$$

for D plasma ($T_i = T_e$). The condition that the stochastic layer reach the axis can be obtained, approximately, from Fig.3 as $\tilde{B}_n \sim 0.033$. Combining these relations we have the condition that the stabilization takes place before the stochastic layer reaches the axis (i.e., partial temperature collapse) as

$$2 s^{2/5} \varepsilon^{-4/5} R_m^{-6/5} n_{20}^{-4/5} T_{keV}^{-1/5} B_T^{2/5} < 1 \qquad (3\text{-}28)$$

An equality on the right gives the crossing of curves (2) and (4) in the parameter space of Fig.3. The higher density case tends to show a partial temperature collapse (curve (4) lying below curve(2) compared to the low density case (curve (4) lying above curve(2)), assuming that the other parameters are equal.

The third example is shown in Fig.7, corresponding to case [III]. We take the same parameters as in Fig.6, except that $B_{ni} = 10^{-5}$ and $\tau_{r0} = 5 \times 10^{-4}$. The mode reaches a full magnetic reconnection. The maximum $\iota(0)$ during the period is close to 1.2, and stochasticity appears during the growing phase of the magnetic perturbation.

The fourth example is shown in Fig.8 for the case of [IV]. The parameters are the same as in Fig.5, except that $B_{ni} = 10^{-5}$ and $\tau_{r0} = 2 \times 10^{-3}$. Since the maximum value of $\iota(0)$ is 1.14 in this

case, the stochasticity does not play an important role in this situation. Comparing type [IV] to type [III], in which the full magnetic reconnection occurs involving the magnetic field stochasticity, the path in parameter space does not show a qualitative difference. The sawtooth crash time, however, will be much shorter in type [III] than in type [IV]. The trigger of the magnetic perturbation is also seen in type [III] but not for type [IV].

The parameter dependence for the appearance of type [III] and [IV] can be understood by the competition between the resistive growth and resistive increment of the shear. If we use Eq.(3-21) and the resistive form $\tau_r \varepsilon_A = s^{2/3} S^{-1/3}$ [4], we have the relation between $\tilde{B}_n$ and s after the crash as

$$\tilde{B}_n = B_{ni} \exp\{(3/56)\varepsilon^{-2} S^{2/3} s^{14/3}\} \qquad (3\text{-}29)$$

From Fig.3, we see that stochasticity does not appear if $\tilde{B}_n$, given Eq.(3-29), is larger than 0.02 at s=0.16, i.e., if the mode reaches the axis before the current layer becomes stochastic. This holds, if the condition

$$1.9\times10^{-5} \varepsilon^{-2} S^{2/3} > \ln(0.02/B_{ni}) \qquad (3\text{-}30)$$

is satisfied. An increase in magnetic Reynolds number S then takes the trajectory from case [III] to case [IV].

To visualize the processes discussed above, we sketch possible paths for sawtooth oscillations in the parameter space of

Fig.3 in Fig.9. Four curves are drawn, labeled by I through IV, corresponding to the four cases. Curves [I]-[III] have three parts labelled by A, B, and C. On A the mode grows slowly with the resistance being classical. The increasing shear, due to the classical transport also occurs on a slow time scale. On B the electron viscosity arising the stochasticity is felt, leading to explosive growth of the perturbation followed by saturation due to the enhanced viscosity. On C the saturated mode partially decays and flux redistribution leads to a state at the initial lower value of shear from which the process repeats itself. Curve [IV] has basically two parts labelled A' and C'. The mode amplitude grows until the X-point and the original magnetic axis merge and disappear. On C', the magnetic flux redistribution leads to a topologically new symmetric state, from which the process repeats itself.

§4 Conclusions and Discussions

In this paper we have demonstrated that stochastization of field lines, resulting from the interaction of the fundamental m/n=1/1 helical mode with other periodicities, plays an important role in sawtooth oscillations. The time scale for the stochastic temperature diffusion has been determined. It was shown to be sufficiently fast to account for the fast sawtooth crash, and is generally shorter than the time scales for the redistribution of current. The enhancement of the electron and ion viscosity, arising from the stochastic field lines, has been calculated. The enhanced electron viscosity always leads to an initial increase in the growth rate of the mode; the enhanced ion viscosity can ultimately lead to mode stabilization before a complete temperature redistribution or flux reconnection has occurred.

A dynamical model has been introduced to calculate the path of the sawtooth oscillation through a parameter space of shear and amplitude of the helical perturbation. The stochastic trigger to the enhanced growth rate and the stabilization by the ion viscosity are also included in the model. A reasonable prescription for the flux reconnection at the end of the growth phase allows us to determine the initial q-value for the successive sawtooth ramps.

Types of Sawtooth Oscillation Our model predicts that four types of the sawtooth oscillations are possible even for a plasma with a monotonic q(r) profile. It is found that the collapse of the central electron temperature does not necessarily mean that a

full reconnection of the magnetic flux occurs.

There are two types of rearrangement of the magnetic configuration, namely:

(M-1) In the case of partial-magnetic reconnection, the q(0) values oscillates around 0.7, and the oscillation amplitude is small (an example in Sec.3 gives $\delta q(0) \sim 0.05$).

(M-2) In the case of full magnetic reconnection, the minimum q(0) value is close to unity. Roughly speaking, q(0) oscillates in the range of 1 and (say) 0.8.

The temperature on the axis can show three classes, namely:

(T-1) Temperature on the axis $T_e(0)$ does not show a sudden collapse. Rapid temperature rearrangement is limited to an annulus near the q=1 rational surface, which then gradually propagates to the axis.

(T-2) $T_e(0)$ is subject to rapid decay, when the stochastic region invades the geometrical axis, before the magnetic island reaches the axis. (The magnetic perturbation either saturates after the stochastic region touches the geometrical axis, or grows to a full reconnection.)

(T-3) $T_e(0)$ collapses because there is a full magnetic reconnection, but the collapse is slow without stochasticity.

Time Scales In our dynamic model of the sawtooth cycles, there are four typical phenomena that occurs during a cycle, each with a time scale for the change of magnetic field: (1) the slow mode growth below the stochastic criterion; (2) the switch on of the stochasticity and rapid growth of the magnetic perturbation; (3) the reconnection process; and (4) the decay of the helical

structure after the mode stops growing.

The first process is no different from conventional models. The second process results in a sudden growth of the helical perturbation, which may be associated with the experimentally observed "magnetic trigger." When the parameter $(\tilde{B}_n, s)$ reaches the stochasticity onset criterion, the enhancement of the growth rate is very large, and the enhanced stochasticity and current diffusivity further accelerate the growth rate of the perturbation. The change of the growth rate occurs within $100\tau_A$. We note that the rapid change in growth rate is characteristic of the case of (M-1) and the part of (M-2) in which magnetic stochasticity plays an essential role (i.e., type [III]). This model also predicts that the stochasticity does not affect the growth rate for the situation of (M-2) if q(0) is always close to unity. The magnetic trigger would not be observed in experiments if the full magnetic reconnection occurs without stochasticity.

The time scale of the temperature collapse, caused by the heat transport across stochastic field lines, has been compared to experimental observations on various machines, and shown to be consistent with those observations. As discussed above, this temperature collapse can be either partial or total, and is not necessarily accompanied by a total field line reconnection.

Stochasticity also can greatly enhance the reconnection process, through the electron viscosity term. The process is the large amplitude phase of the enhanced growth. This fast reconnection allows the hot core to shift on the same time scale as the temperature crash, as observed experimentally. The distinc-

tion between the flattening of the temperature by stochastic diffusion and by fast stochasticity-induced reconnection is therefore not determined by the timescale alone.

Experimental observations could include various combinations of the oscillations discussed above; i.e, Type [I] (M-1,T-1), Type [II] (M-1,T-2), Type [III] (M-2,T-2), and Type [IV] (M-2,T-3). To classify the sawtooth experiments, the temperature crash and magnetic rearrangement must be separately observed. In the case of a partial reconnection, the flattening of the temperature and q(0) below unity after the collapse are observed at the same time. The situation, in which the island stops growing but the stochasticity reaches the axis, occurs more easily for the strong shear case, i.e., low q profiles. The case where $T_e(0)$ has a partial collapse before a full collapse, sometimes called as "compound sawtooth"[14], can occur with a monotonically decreasing q, q(0) remaining below unity.

The lack of correspondence between the numerical codes with q(0) considerably below one [25,26], which show complete reconnections, and experimental observations [13], have lead to consideration of more complicated q-profiles[31]. In particular, the existence of a persistent q=1 island in JET, but with large excursions in radius during the sawtooth (the "snake")[33], has lead to consideration of a q-profile that is flattened near the q=1 surface [22]. Numerical calculations indicate that such profiles are consistent with a partial reconnection [22,35]. However, the recovery phase of the sawtooth (the ramp) is not self-consistent in the calculation. Within the context of our

theoretical picture more complicated q-profiles are certainly possible. While they are not necessary to qualitatively explain many of the observations, they may be necessary to explain the motion of the "snake".

Although the effect of field fluctuations in modifying the transport coefficients has long been known, it is only recently that the effect has been used in toroidal codes[30]. It is clear from our study that it is most important to do so. This will ultimately allow for the treatment of the decay phase of islands after an incomplete reconnection, and can also bear on the time evolution of the shape of the q-profile. An important diagnostic for such codes would be the shapes of the hot and cold regions. Recent developments in the experimental observations have made possible the determination of the shapes of these regions. For example, a Kadomtsev type reconnection, which has not been thought to predict the 'hot crescent', was found to lead to a situation in which the hot core is distorted into a crescent when more elaborate computations were made[26]. A similar full computation could determine the shape of the cross sections of the hot and cold regions including the stochasticity.

It has recently been suggested that inertial effects can play a role in a fast reconnection [36]. If stochasticity is present, then additional inertial effects are not necessary to explain the observation. Inertial effects might be distinguished by the time scale of a low shear reconnection for which stochasticity is not important.

The analysis of the stabilization by the ion viscosity is

based on a perturbation treatment. More thorough study is necessary to investigate quantitatively the reduction of the growth rate in the large viscosity cases. This would improve approximate stability criterion (3-27). The final decay phase of the helical configuration is not completely analyzed in this paper. When the mode is marginally stable, the temporal change is much slower than the characteristic mode growth rate. Experimental observations on the decay of the postcursor have reported that the postcursor damps with the time scale of a few (or few tens) of milliseconds. When the linear mode growth is greatly reduced, the nonlinear coupling to higher m-modes may take away mode energy. The higher m-modes are more easily damped by the ion viscosity. These problems await future analysis.

Acknowledgements

This work was performed during one of the authors (AJL) visit to the National Institute for Fusion Science as visiting professor on the Joint Institute for Fusion Theory US-Japan exchange program. He also acknowledges discussions with Dr. A. Boozer. The authors acknowledge discussions with Drs. S. Tsuji, D. Campbell, and J. A. Wesson on experimental observations of sawtooth phenomena. This work is partly supported by the Grant-in-Aid for Scientific Research of MoE Japan.

Appendix A1 Transport coefficient in the presence of magnetic stochasticity

We briefly outline the derivation of the electron thermal diffusivity, current resistivity and ion viscosity in the presence of magnetic stochasticity. The electron thermal diffusivity and the current viscosity have been discussed in literature. We follow the argument by Boozer for this problem [29].

The kinetic equation for electrons in the presence of magnetic stochasticity can be written as

$$\frac{\partial f}{\partial t} + v\cdot\nabla f + \frac{q}{m}(E+v\times B)\cdot\nabla_v f = \frac{\partial}{\partial x}\left(|v_{//}|D_M\right)\frac{\partial f}{\partial x} + C(f) \qquad (A1\text{-}1)$$

where C is a collision operator and D_M indicates the diffusivity of the magnetic field line in the presence of stochasticity.

We assume that f is close to Maxwellian and is estimated by the shifted Maxwellian distribution. In order to obtain the electron thermal diffusivity, we calculate

$$\frac{\partial}{\partial x}\left[\int\frac{1}{2}mv^2|v_{//}|D_M\frac{\partial f}{\partial x}d^3v\right]. \qquad (A1\text{-}2)$$

Writing this term as $(\partial/\partial x)[n\chi_e\partial T/\partial x]$ (where x is the direction of the gradient of the distribution, the z-axis is taken in the

direction of the ensemble-averaged magnetic field), and evaluating the integral, we have [29]

$$\tau_e = (3/\sqrt{\pi})v_{Te}D_M \ . \qquad \text{(A1-3)}$$

The equation for the current diffusivity is obtained by setting $\partial f/\partial v_{//} = -(mv_{//}/T)f$ in Eq.(A1-1), multiplying by $qv_{//}/|v_{//}|$ and integrating over the velocity space. This gives the necessary electric field to balance the current viscosity as [29]

$$-E_z\int(q^2|v_{//}|f_M d^3v)/T = \frac{\partial}{\partial x}D_M\frac{\partial J_z}{\partial x} \qquad \text{(A1-4a)}$$

or

$$E_z = -\frac{\partial}{\partial x}\left[\frac{TD_M}{\int q^2|v_{//}|f_M d^3v}\right]\frac{\partial J_z}{\partial x} \ . \qquad \text{(A1-4b)}$$

Dropping the inertia terms, the parallel component in Ohm's law can be written

$$E_z + (v\times B)_z = \eta J_z - \lambda\nabla^2 J_z \qquad \text{(A1-5)}$$

where η is the classical resistivity, and λ is to be determined from (A1-4). Evaluating the integrals in A1-4[29],

$$\lambda = \frac{\sqrt{\pi}}{2}\mu_0 \frac{c^2}{\omega_p^2} v_{Te} D_M \ . \qquad \text{(A1-6)}$$

The ion shear viscosity can be obtained in a similar manner. Operating on Eq.(A1-1) with the integral $\int m_i v_y d^3v$, we have the equation of the motion in the y-direction as

$$m_i \frac{\partial}{\partial t} n V_y + m_i n v \cdot \nabla V_y + qn(E+v\times B)_y = \frac{\partial}{\partial x}\int m_i v_y (|v_{//}| D_M \frac{\partial f}{\partial x} d^3v \qquad \text{(A1-7)}$$

where V_y is the fluid velocity in the y-direction and the collisional drag force by electrons has been neglected. Evaluating the velocity integral we have

$$\int m_i v_y |v_{//}| (\partial f/\partial x) d^3v = m_i n_i (v_{Ti}/\sqrt{\pi}) D_M (\partial V_y/\partial x). \qquad \text{(A1-8)}$$

The viscous force is given as

$$F_y = (\partial/\partial x) m_i n_i (v_{Ti}/\sqrt{\pi}) D_M (\partial V_y/\partial x). \qquad \text{(A1-9)}$$

Writing the viscous force as

$$F_y = \nabla m_i n_i \mu_i \nabla V_y, \qquad \text{(A1-10)}$$

we have

$$\mu_i = (v_{Ti}/\sqrt{\pi})D_M. \qquad \text{(A1-11)}$$

Comparing Eqs.(A1-3) and (A1-6), we have the relation

$$\lambda/\chi_e = \frac{\pi}{6}\mu_0\frac{c^2}{\omega_p^2} \quad . \qquad \text{(A1-12)}$$

Comparing Eq.(A1-3) and (A1-11) we have

$$\mu_i/\chi_e = v_{Ti}/3v_{Te}. \qquad \text{(A1-13)}$$

Appendix A2 Growth rate of magnetic perturbation in the presence of stochastic plasma transport.

The linear growth rate of the m/n=1/1 mode has been extensively discussed in the literature. Following the argument of Aydemir [30], in which the current diffusivity λ is included, we evaluate the linear growth rate, in the presence of additional ion viscosity μ_i. The linear mode growth rate is derived by the linearlized reduced set of equations as [30]

$$\frac{\partial \tilde{\Phi}}{\partial t} + \nabla_{//} \tilde{J} = \mu_i \nabla^2 \tilde{\Phi} \qquad \text{(A2-1)}$$

$$\frac{\partial \tilde{\psi}}{\partial t} + \nabla_{//} \tilde{U} = \eta \tilde{J} - \lambda \nabla^2 \tilde{J} \qquad \text{(A2-2)}$$

where the quantities $\tilde{U}$ and $\tilde{J}$ indicates the stream function and parallel current of the m/n=1/1 component, $\tilde{J}=\nabla^2\tilde{\psi}$ and $\tilde{\Phi}=\nabla^2\tilde{U}$.

We study the effect of the ion viscosity in a perturbative manner. We employ an order-of-magnitude estimate to evaluate the ion viscosity damping term in Eq.(A2-1). The stream function and vorticity $\tilde{\Phi}$ change rapidly near the mode rational surface. The characteristic scale length of this change, w, which is much shorter than the minor radius of the rational surface, is derived

in Ref.[30]. Using this value we estimate the right hand side of Eq.(A2-1) as

$$\mu_i \nabla^2 \tilde{\Phi} = -\mu_i \tilde{\Phi}/w^2. \qquad \text{(A2-3)}$$

The eigenmode analysis gives the rewritten form of (A2-1), in the absence of the ion viscosity, as [30]

$$\partial\tilde{\Phi}/\partial t - \tau_0 \tilde{\Phi} = 0 \qquad \text{(A2-4)}$$

Adding the ion viscosity damping perturbatively, this relation becomes

$$\partial\tilde{\Phi}/\partial t - \tau_0 \tilde{\Phi} = -\mu_i \tilde{\Phi}/w^2, \qquad \text{(A2-5)}$$

such that the new growth rate is

$$\tau_s = \tau_0 - \mu_i/w^2. \qquad \text{(A2-6)}$$

The mode growth rate τ_0 and the thickness w were derived, where the m/n=1/1 MHD mode is stable, as[30]

$$\tau_0 \left(\frac{R}{v_A}\right) \simeq 5(2\varepsilon s)^{4/5} \left[\frac{\lambda}{\mu_0 r_1^4} \frac{R}{v_A}\right]^{1/5} \qquad \text{(A2-7)}$$

and

$$\frac{w}{r_1} = (2\varepsilon s)^{-1/3}\left[\frac{\lambda}{\mu_0 r_1^4}\frac{R}{v_A}\right]^{1/6}\cdot\left[\tau_0\frac{R}{v_A}\right]^{1/6}. \qquad \text{(A2-8)}$$

Substituting Eqs.(A2-7) and (A2-8) into Eq.(A2-6), we have

$$\tau_s = \tau_0 - 5^{-1/3}\frac{\mu_i}{r_1^2}(2\varepsilon s)^{2/5}\left[\frac{\lambda}{\mu_0 r_1^4}\frac{R}{v_A}\right]^{-2/5} \qquad \text{(A2-9)}$$

where the suffix s indicates the enhancement by the magnetic stochasticity. If we use the relation that

$$\mu_i/\lambda = \frac{2v_{Ti}}{\pi v_{Te}}\cdot\frac{\omega_p^2}{\mu_0 c^2} \qquad \text{(A2-10)}$$

in (A2-9), and substituting for τ_0 from (A2-7), we have

$$\tau_s\left(\frac{R}{v_A}\right) = 5(2\varepsilon s)^{4/5}\left[\frac{\lambda}{\mu_0 r_1^4}\frac{R}{v_A}\right]^{1/5} - 5^{-1/3}(2\varepsilon s)^{2/5}\cdot\alpha\left[\frac{\lambda}{\mu_0 r_1^4}\frac{R}{v_A}\right]^{3/5}$$

(A2-11)

where the dimensionless coefficient α is given as

$$\alpha = \frac{2v_{Ti}}{\pi v_{Te}} \cdot \frac{\omega_p^2 r_l^2}{c^2} \qquad \text{(A2-12)}$$

Noting the powers of λ in the first and second terms in the right hand side, we see that, when the stochasticity switches on and λ is small, the first term dominates over the second term and accelerates the mode growth. If the stochastic transport coefficient becomes larger, however, the second term can exceed the first one, thus stabilizing the mode.

We note here that the expression Eq.(A2-11) is derived with the assumption that the ion viscosity is treated as a perturbation. The determination of the condition for zero growth rate from Eq.(A2-11) will include some numerical uncertainty. The purpose of the analysis here is not an exact calculation of the growth rate, but to indicate that the stochastic ion viscosity can stabilize the mode.

References

[1] Von Goeler, S.L., Stodiek, W., Sauthoff, N.: Phys. Rev. Lett. **33** (1974) 1201.

[2] McGuire, K., Robinson, D. C.: Nucl. Fusion **19** (1979) 505.

[3] Dubois, M. A., Pecquet, A. L.,Reverdin, C.: Nucl. Fusion **23** (1983) 147.

[4] Coppi, B., Galvao, R., Pellat, R., Rosenbluth, M. N., and Rutherford, P. H.: Sov. J. Plasma Phys. 2 (1976) 533.

[5] Monticello, D. A., White, R.: Nucl. Fusion **16** (1976) 528.

[6] Sykes, A, Wesson, J. A.: Phys. Rev. Lett. **37** (1976) 140.

[7] Holmes, J. A., Carreras, B. A., Hicks, H. R., Lynch, V. E., Rothe K. E.: Phys. Fluids **25** (1982) 800; and Tanaka, Y., Azumi, M., Kurita, G., Takeda, T.: Plasma Phys. Cont. Fusion **27** (1985) 579.

[8] Jahns, G. L., Soler, M., Waddel, B. V., Callen J. D., Hicks, H. R.: Nucl. Fusion **18** (1978) 735.

[9] Dubois, M. A., Samain, A.: Nucl. Fusion **20** (1980) 1101.

[10] Park, W., Monticello, D. A.: Nucl. Fusion 30 (1990) 2431.

[11] Kadomtsev, B. B.; Sov. J. Plasma Phys. 1 (1975) 389.

[12] Campbell, D. J., Gill, R. D., Gowers, C. W., Wesson, J. A., Bartlett, D. V., et al.: Nucl. Fusion **26** (1986) 1085.

[13] Campbell, D. J., Duperrex, P. A., Edwards, A. W., Gill, R. D., Gowers, C. W., et al.: *Plasma Physics and Controlled Nuclear Fusion Research 1986*, Proc. 11th Int. Conf. on Plasma Phys. and Controlled Fusion, IAEA, (1987) Vol.1, 433; Campbell, D. J., Cordey, J. G., Edwards, A. W., Gill, R. D.,

Lazzaro, E., et al.: *Plasma Physics and Controlled Nuclear Fusion Research 1988*, Proc. 12th Int. Conf. on Plasma Phys. and Controlled Fusion, IAEA, (1989) Vol.1, 377.

[14] McGuire, K., Arunasalam, V., Bell, M. G., Bitter, M., Blanchard, W. R., et al: *Plasma Physics and Controlled Nuclear Fusion Research 1986*, Proc. 11th Int. Conf. on Plasma Phys. and Controlled Fusion, IAEA, (1987) Vol.1, 421.

[15] Wesson, J. A.: *Plasma Physics and Controlled Nuclear Fusion Research 1986*, Proc. 11th Int. Conf. on Plasma Phys. and Controlled Fusion, IAEA, (1987) Vol.2, 3.

[16] Rosenbluth, M. N., Sagdeev, R. Z., Taylor, J. B., Zaslavsky, G. M.: Nucl. Fusion **6** (1966) 297.

[17] Finn, J. M.: Phys. Fluids **20** (1977) 1749.

[18] Carreras, B., Hicks, H. R., Lee, D. K.: Phys. Fluids **24** (1981) 66.

[19] Fries, R. P., Hartman, C. W., Hamzeh, F. M., Lichtenberg, A. J.: Nucl. Fusion **13** (1973) 533.

[20] Rechester, A. B., Stix, T. H.: Phys. Rev. lett. **36** (1976) 587.

[21] Lichtenberg, A. J.: Nuclear Fusion 24 (1984) 1277.

[22] Soltwisch, H., Stodiek, W., Manikam, J., Schluter, J.: *Plasma Physics and Controlled Nuclear Fusion Research 1986*, Proc. 11th Int. Conf. on Plasma Phys. and Controlled Fusion, IAEA, (1987) Vol.1, 263.

[23] JET Team: *Plasma Physics and Controlled Nuclear Fusion Research 1986*, Proc. 11th Int. Conf. on Plasma Phys. and Controlled Fusion, IAEA, (1987) Vol.1, 499.

[24] West, W. P., Thomas, D. M., de Grassie, J. S.: Phys. Rev. Lett. **58** (1987) 2758.

[25] Izzo, R. Monticello, D. A., Stodiek, W., and Park, W.: Phys. Fluids **30** (1987) 1442.

[26] Aydemir, A. Y., Wiley, J. C., and Ross, D. W.: Phys. Fluids **B1** (1989) 774.

[27] Lichtenberg, A. J., Lieberman M. A.: *Regular and Stochastic Motion*, Springer Verlag, (1984) Sec. 4.2.

[28] Kaw, P., Valeo, E. J., Rutherford, P. H.: Phys. Rev. Lett. **43** (1979) 1398.

[29] Boozer, A.: J. Plasma Phys. **35** (1986) 133; and private communication (1986).

[30] Aydemir, A. Y.: Phys. Fluids **B2** (1990) 2135.

[31] White, R. B.: *Theory of Tokamak Plasmas* (North Holland, Amsterdam, 1989) §6.9.

[32] Holmes, J. A., Carreras, B. A., Charlton, L. A.: Phys. Fluids **B1** (1989) 788.

[33] Weller, A., Cheetham, A. D., Edwards, A. W., Gill, R. D., Gondhalekar, A., et al. : Phys. Rev. Lett. **59** (1987) 2303.

[34] JET Team: *Plasma Physics and Controlled Nuclear Fusion Research 1986*, Proc. 11th Int. Conf. on Plasma Phys. and Controlled Fusion, IAEA, (1987) Vol.1, 31.

[35] Rogister, A., Kaleck, A., Psimopoulos, M., Hasselberg, G.: Phys. Fluids B2 (1990) 953.

[36] Wesson, J. A.: *Plasma Physics and Controlled Nuclear Fusion Research 1990*, 13th Int. Conf. on Plasma Phys. and Controlled Fusion, IAEA, (1990) paper IAEA-CN-53/I-1-4.

Figure Captions

Fig.1 Model Tokamak Geometry. Coordinates and the location of the mode rational surface (q=1) are shown in (a). Magnetic island and the stochasticity region (hatched region) are illustrated in (b). Δr, δ_S and δ_X indicate the width of the main magnetic island, the thickness of the stochastic layer near the O-point, and that near the X-point, respectively.

Fig.2 Overlapping of secondary magnetic island around the m/n=1/1 fundamental island as a function of the normalized magnetic perturbation amplitude, $\tilde{B}_n$, at the poloidal angle (a) of the O-point and (b) X-point. (s=0.6). Hatched region indicates the stochasticity layer. Main magnetic island separatrix is shown by the dotted line in (a).

Fig.3 Domains of stochasticity and reconnection on the s-$\tilde{B}_n$ plane. The upper solid line (1) shows the condition for full reconnection, i.e. the magnetic island reaches the geometrical axis. The lower solid line (2) indicates the condition that the stochastic layer reaches the geometrical axis. The lower dashed line (3) indicates the boundary, above which stochasticity enhances the mode growth. The upper dashed line (4) shows the criterion for mode stabilization by ion viscosity.

Fig.4 Typical examples of the magnetic configurations. Symbols

A, B and C correspond to those in Fig.3. The dashed lines are the boundaries of the stochastic regions, and the solid lines the separatrices.

Fig.5 Example of the temporal evolution for case [I], partial magnetic reconnection and partial temperature crash. Development of s and $\tilde{B}_n$ are shown in (a) and (b). The decay phase, shown by a dotted line, does not include a time scale. An expanded time scale is shown in (c) for the magnetic perturbation and in (d) for the radial location of stochasticity boundary (at 0-point, see Fig.2(a)), near the crash time. Parameters are: $\varepsilon=0.1$, $\alpha=1800$, $\Gamma_0=7\times10^{-5}$, $\tau_{r0}=10^{-5}$, $\rho=10^{-7}$ and $B_{ni}=10^{-3}$.

Fig.6 Example of the temporal evolution for case [II], partial magnetic reconnection and central temperature crash. Development of s and $\tilde{B}_n$ are shown in (a) and (b). The evolution of the magnetic perturbation and stochastic layer are shown in (c) and (d) with an expanded times scale, near the collapse time. It is seen that the stochastic region reaches the geometrical axis. Parameters are the same as in Fig.5 except $\Gamma_0=8.95\times10^{-5}$ and $\alpha=1130$.

Fig.7 Example of the temporal evolution for case [III], full magnetic reconnection and central temperature crash; the stochasticity enhances the mode growth. Development of s and $\tilde{B}_n$ are shown in (a) and (b). Expanded time scale is

shown in (c) and (d) near the crash time. Parameters are the same as in Fig.6 except $\tau_{r0}=5\times10^{-4}$ and $B_{ni}=10^{-5}$.

Fig.8 Example of the temporal evolution for case [IV], full magnetic reconnection and central temperature crash; the stochasticity does not enhance the mode growth. Parameters are the same as in Fig.5 except $\tau_{r0}=2\times10^{-3}$ and $B_{ni}=10^{-5}$.

Fig.9 Schematic examples of the trajectories of the dynamical evolution. The four cases [I] to [IV] are illustrated. In case [I], the slow evolution first follows A, the rapid growth follows B; relaxation closes the cycle on C. In case [II], the stochastic region touches the geometrical axis and the central temperature crashes before the mode stops growing. In case [III], there is a full collapse after the triggering of the fast growth, without mode stabilization. In case [IV], stochasticity does not play an important role.

Table 1 The classification of the sawtooth oscillations.

	Magnetic Field Stochasticity	
	Important	Not
Magnetic Collapse / Temperature Collapse	Partial	Full
Partial	I	----	----
Full	II	III	IV

Fig. 1

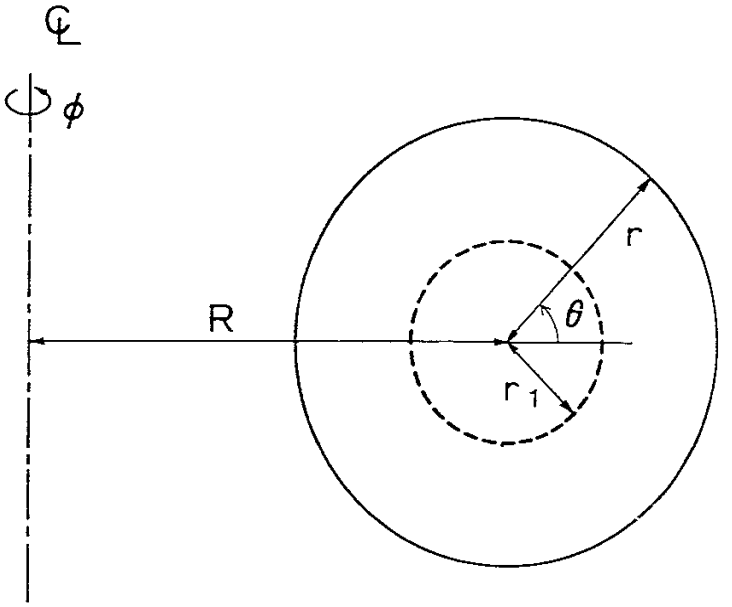

(a)

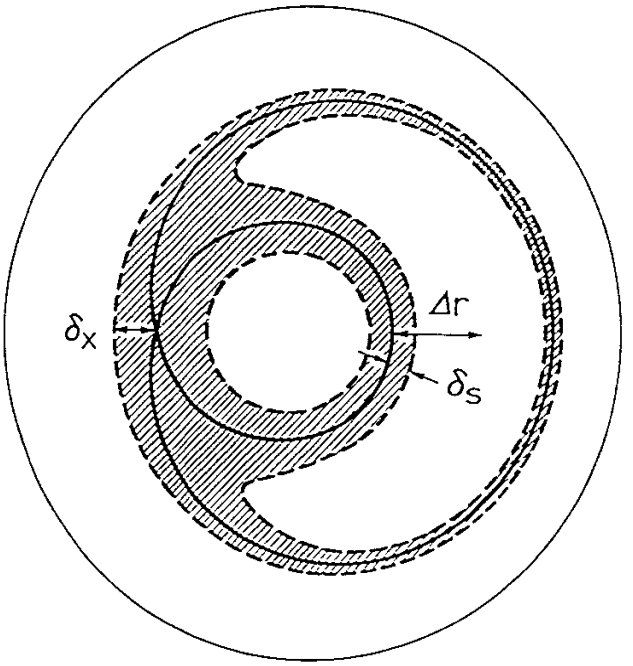

(b)

Fig. 2

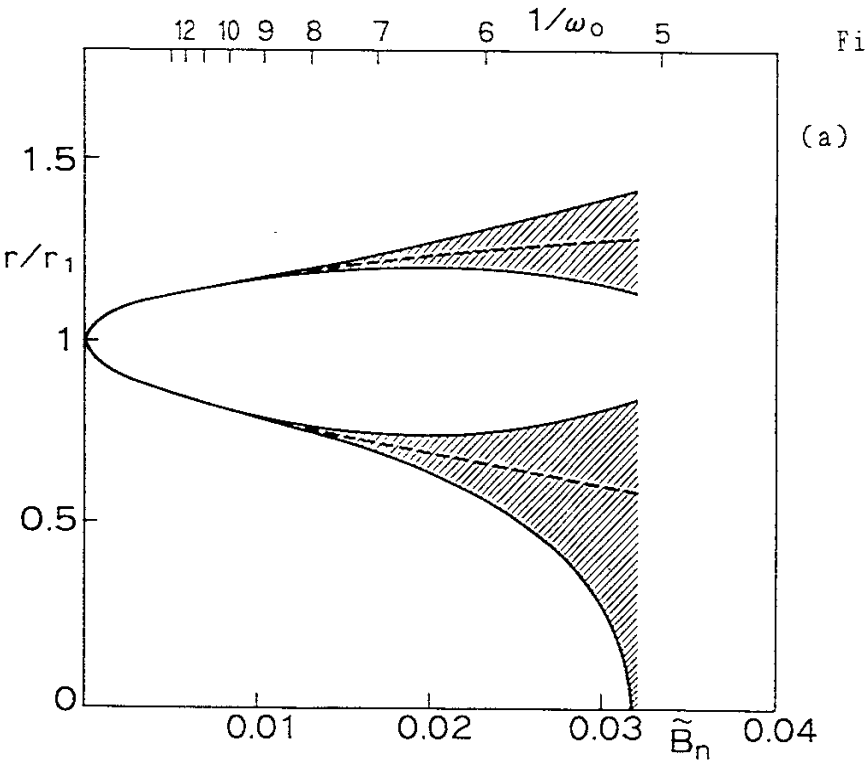
12 10 9 8 7 6 1/ω₀ 5
(a)
1.5
r/r₁
1
0.5
0
0.01 0.02 0.03 B̃n 0.04

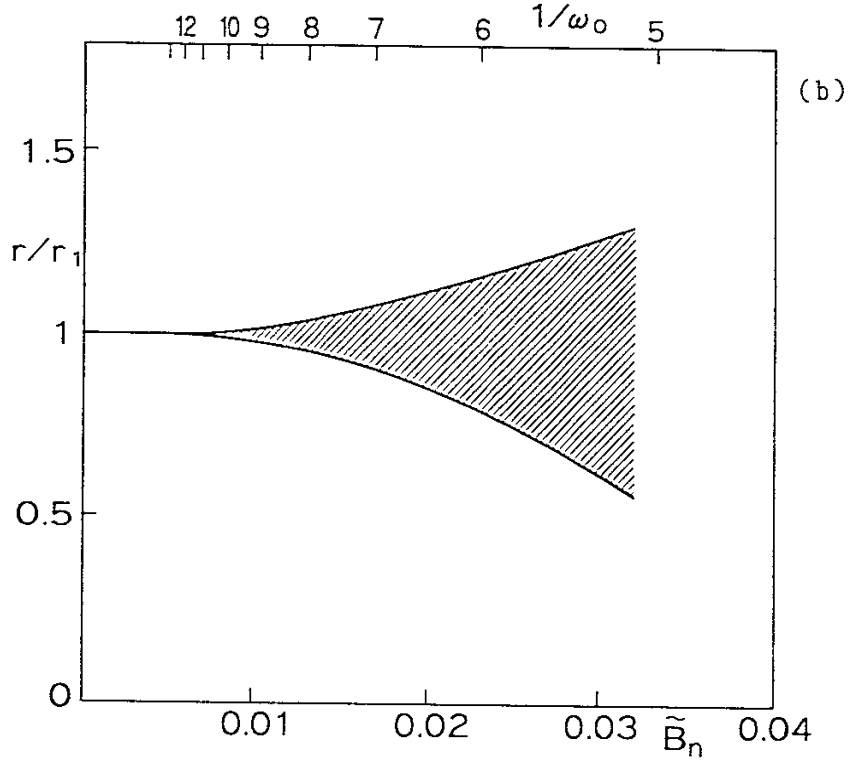
12 10 9 8 7 6 1/ω₀ 5
(b)
1.5
r/r₁
1
0.5
0
0.01 0.02 0.03 B̃n 0.04

Fig. 3

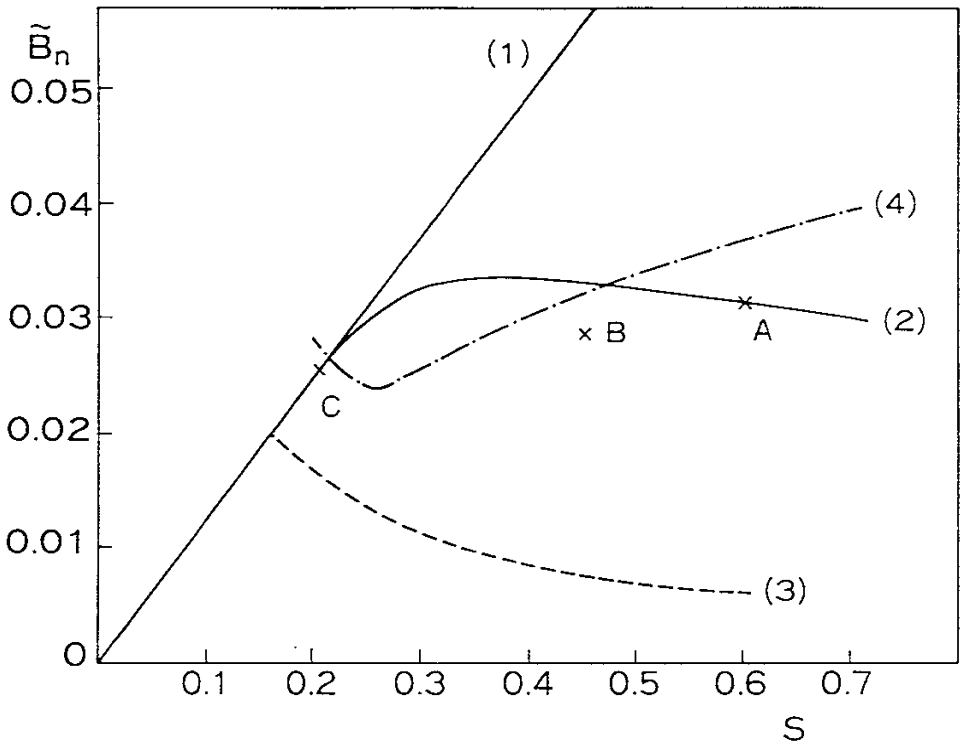

Fig. 4

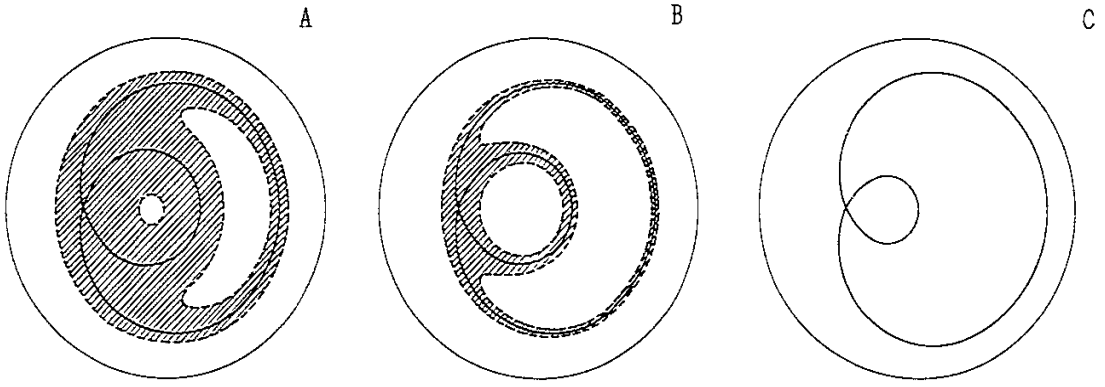

Fig. 5

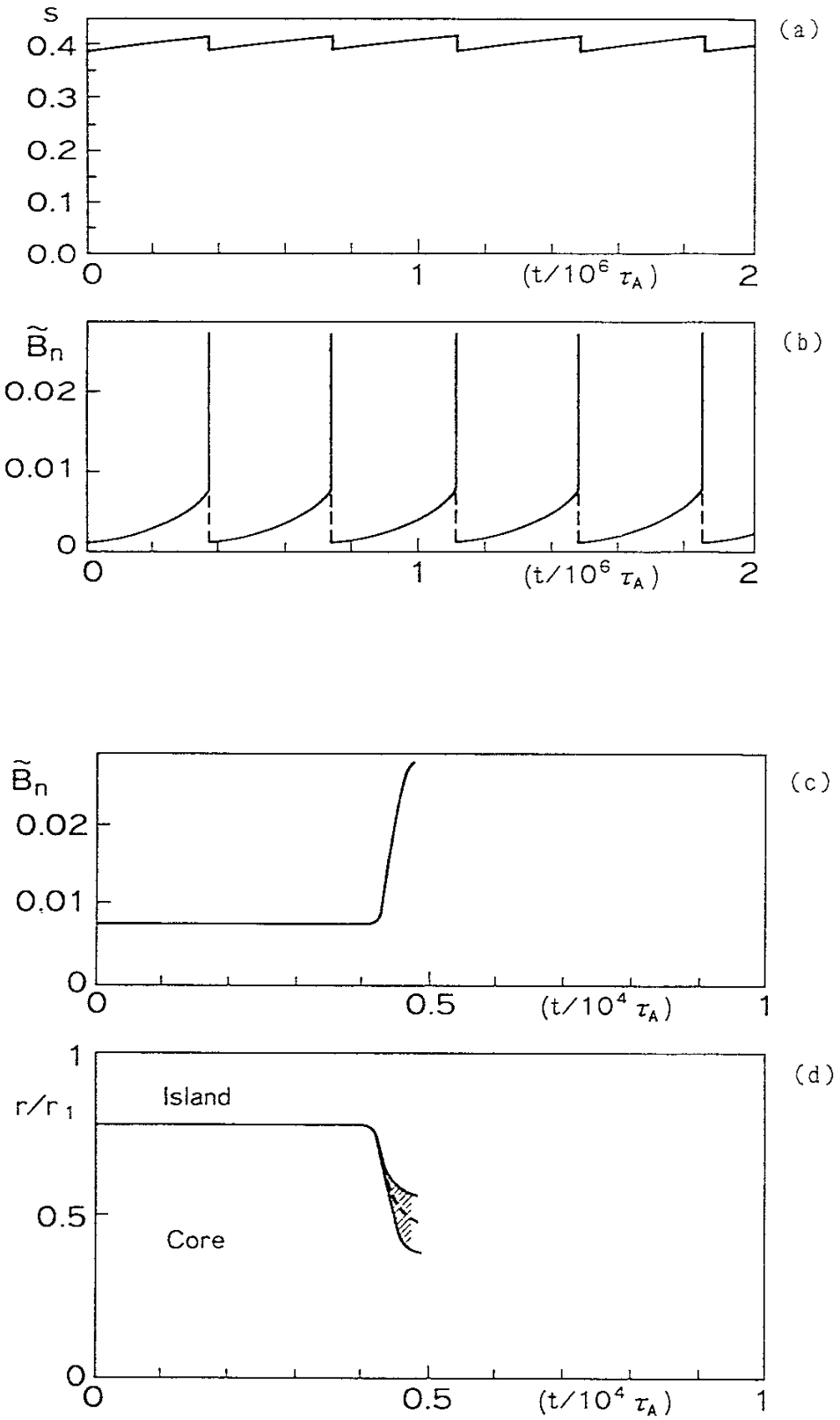
s
0.4
0.3
0.2
0.1
0.0
0
1
(t/10^6 τA)
2
(a)
B̃n
0.02
0.01
0
0
1
(t/10^6 τA)
2
(b)
B̃n
0.02
0.01
0
0
0.5
(t/10^4 τA)
1
(c)
1
r/r1
Island
Core
0.5
0
0
0.5
(t/10^4 τA)
1
(d)

Fig. 6

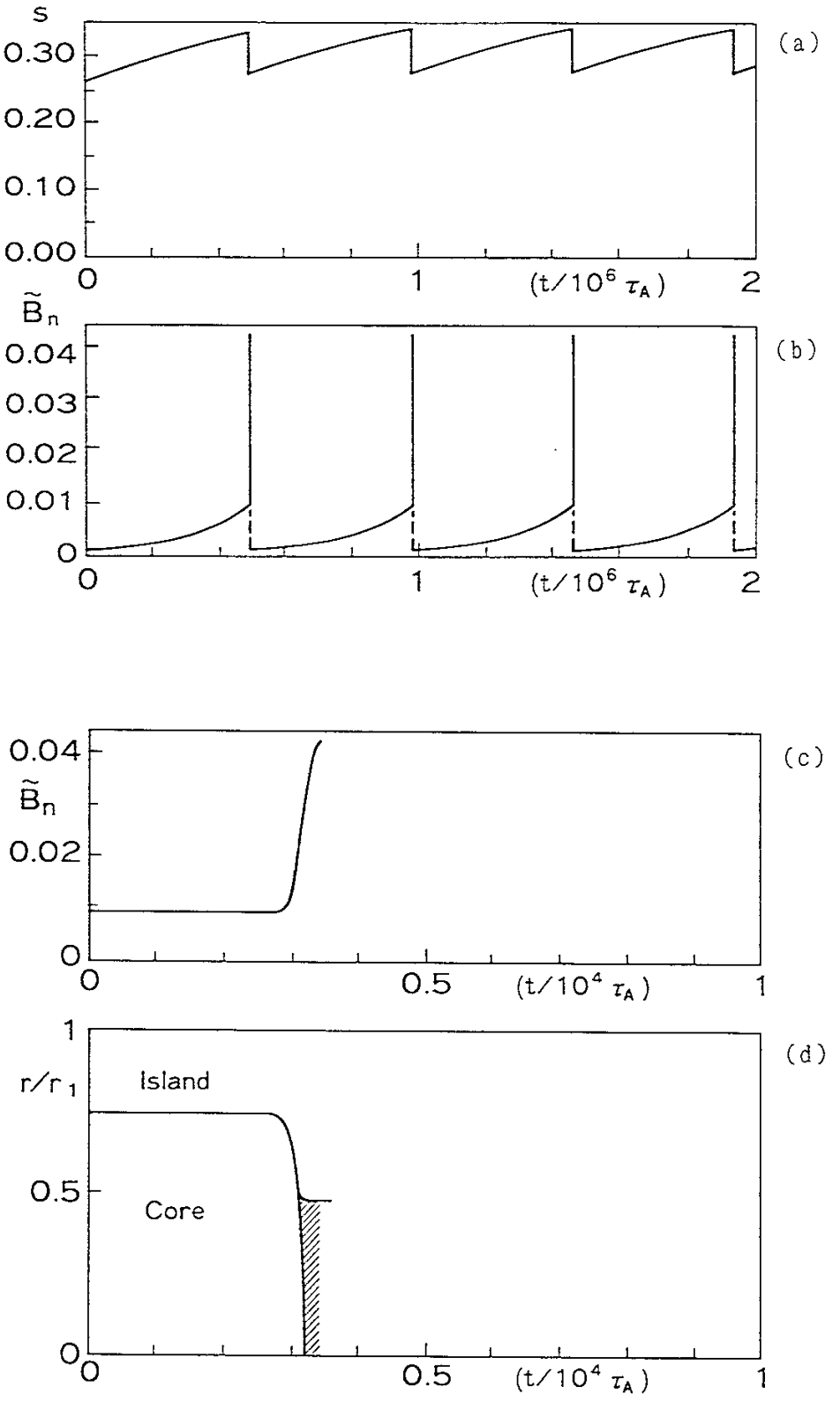
s
0.30
0.20
0.10
0.00
0
1
(t/10^6 τA)
2
(a)
B̃n
0.04
0.03
0.02
0.01
0
0
1
(t/10^6 τA)
2
(b)
0.04
B̃n
0.02
0
0
0.5
(t/10^4 τA)
1
(c)
1
r/r1
Island
0.5
Core
0
0
0.5
(t/10^4 τA)
1
(d)

Fig. 7

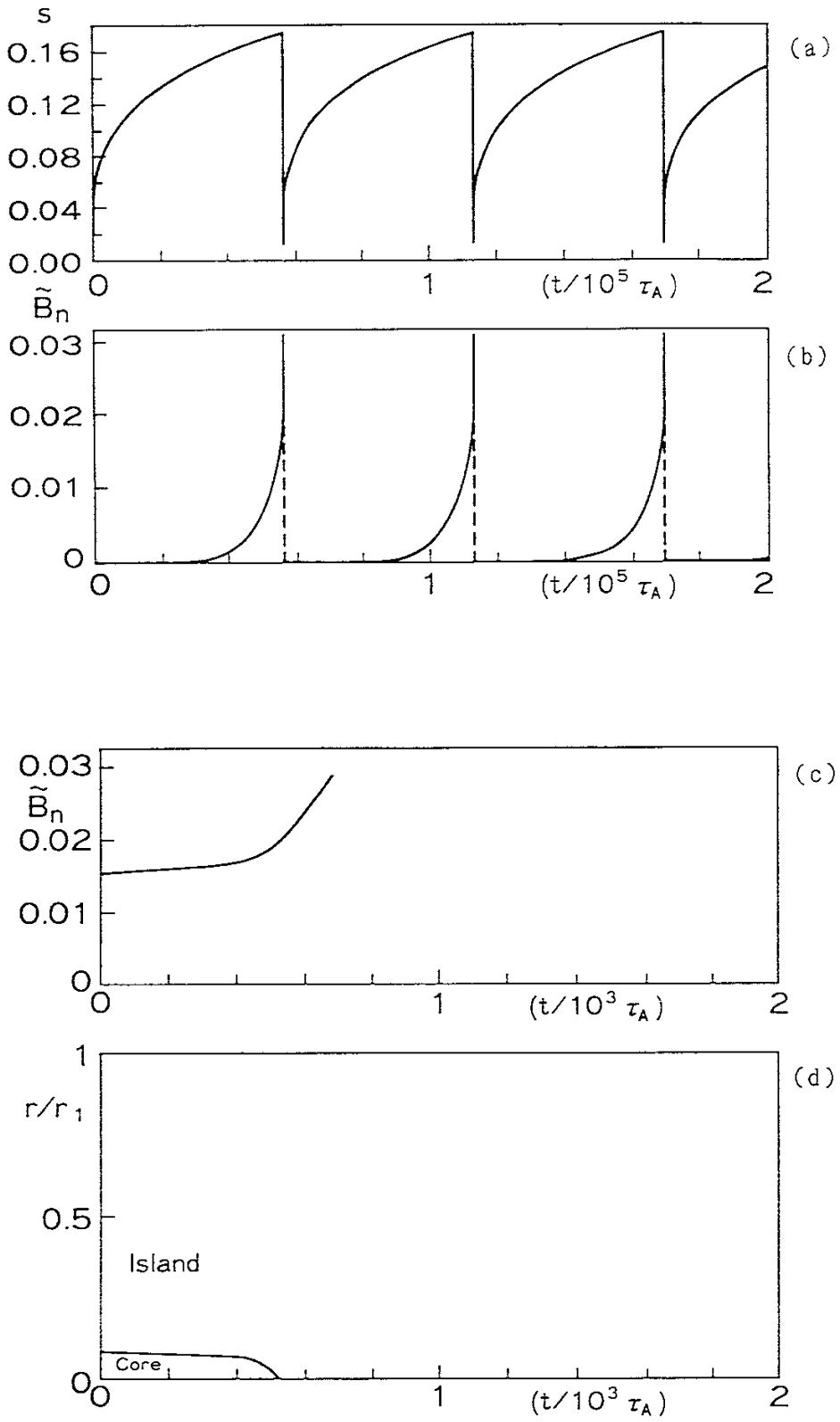
s
0.16
0.12
0.08
0.04
0.00
0
1
(t/10^5 τA)
2
(a)
B̃n
0.03
0.02
0.01
0
0
1
(t/10^5 τA)
2
(b)
0.03
B̃n
0.02
0.01
0
0
1
(t/10^3 τA)
2
(c)
1
r/r1
0.5
Island
Core
0
0
1
(t/10^3 τA)
2
(d)

Fig. 8

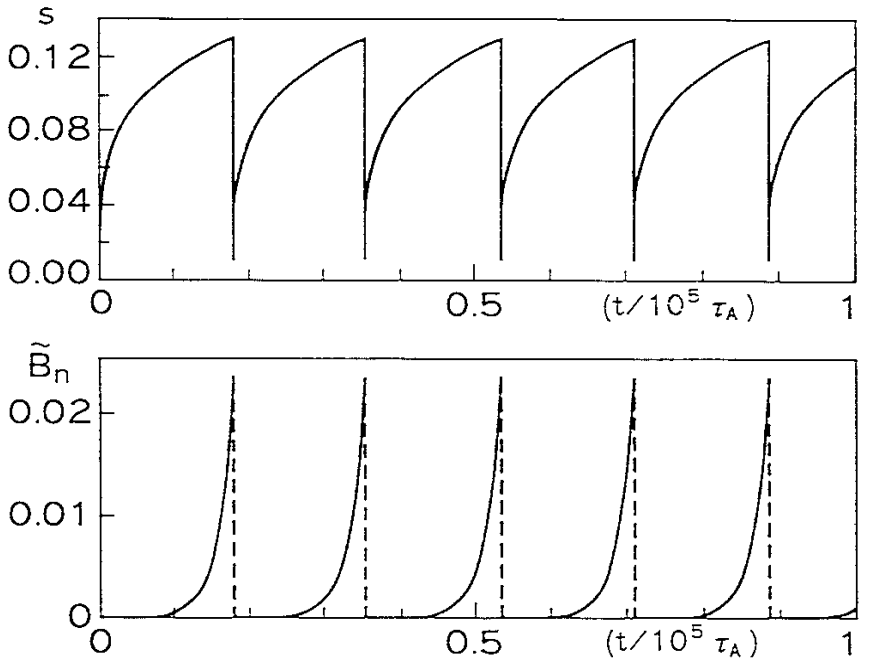

Fig. 9

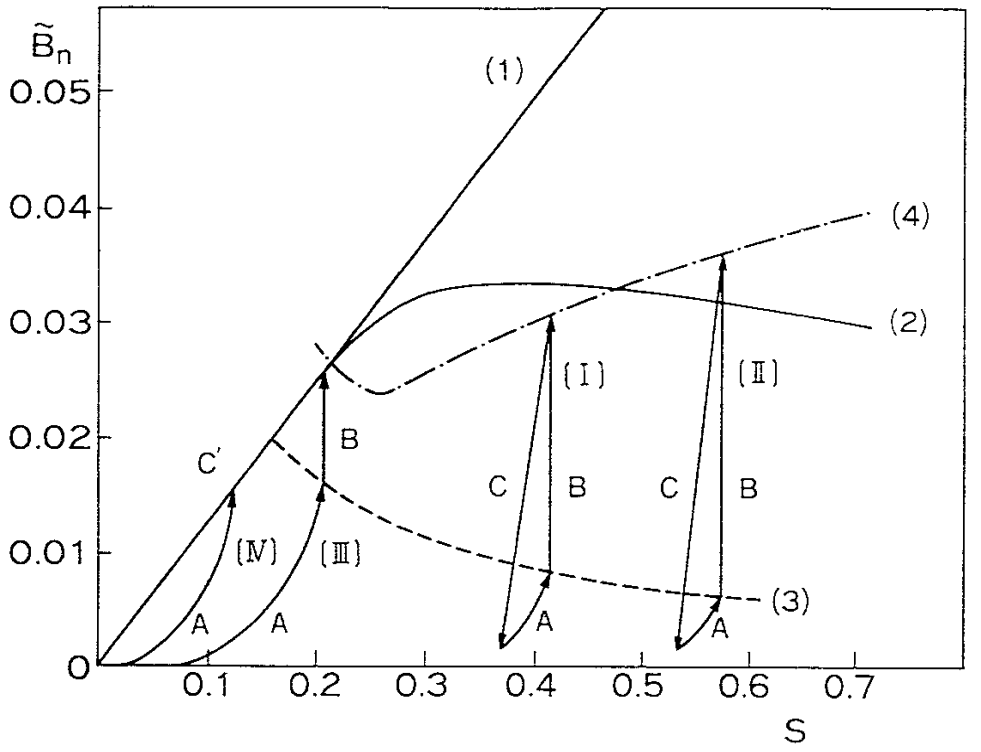
$\tilde{B}_n$
0.05
0.04
0.03
0.02
0.01
0
0.1
0.2
0.3
0.4
0.5
0.6
0.7
S
(1)
(2)
(3)
(4)
C'
B
C
B
C
B
A
A
A
A
〔Ⅰ〕
〔Ⅱ〕
〔Ⅲ〕
〔Ⅳ〕

Recent Issues of NIFS Series

NIFS-46 K.Kusano, T.Tamano and T. Sato, *Simulation Study of Nonlinear Dynamics in Reversed-Field Pinch Configuration*; Sep. 1990

NIFS-47 Yoshi H.Ichikawa, *Solitons and Chaos in Plasma*; Sep. 1990

NIFS-48 T.Seki, R.Kumazawa, Y.Takase, A.Fukuyama, T.Watari, A.Ando, Y.Oka, O.Kaneko, K.Adati, R.Akiyama, R.Ando, T.Aoki, Y.Hamada, S.Hidekuma, S.Hirokura, K.Ida, K.Itoh, S.-I.Itoh, E.Kako, A. Karita, K.Kawahata, T.Kawamoto, Y.Kawasumi, S.Kitagawa, Y.Kitoh, M.Kojima, T.Kuroda, K.Masai, S.Morita, K.Narihara, Y.Ogawa, K.Ohkubo, S.Okajima, T.Ozaki, M.Sakamoto, M.Sasao, K.Sato, K.N.Sato, F.Shinbo, H.Takahashi, S.Tanahashi, Y.Taniguchi, K.Toi and T.Tsuzuki, *Application of Intermediate Frequency Range Fast Wave to JIPP T-IIU Plasma*; Sep.1990

NIFS-49 A.Kageyama, K.Watanabe and T.Sato, *Global Simulation of the Magnetosphere with a Long Tail: The Formation and Ejection of Plasmoids*; Sep.1990

NIFS-50 S.Koide, *3-Dimensional Simulation of Dynamo Effect of Reversed Field Pinch*; Sep. 1990

NIFS-51 O.Motojima, K. Akaishi, M.Asao, K.Fujii, J.Fujita, T.Hino, Y.Hamada, H.Kaneko, S.Kitagawa, Y.Kubota, T.Kuroda, T.Mito, S.Morimoto, N.Noda, Y.Ogawa, I.Ohtake, N.Ohyabu, A.Sagara, T. Satow, K.Takahata, M.Takeo, S.Tanahashi, T.Tsuzuki, S.Yamada, J.Yamamoto, K.Yamazaki, N.Yanagi, H.Yonezu, M.Fujiwara, A.Iiyoshi and LHD Design Group, *Engineering Design Study of Superconducting Large Helical Device*; Sep. 1990

NIFS-52 T.Sato, R.Horiuchi, K. Watanabe, T. Hayashi and K.Kusano, *Self-Organizing Magnetohydrodynamic Plasma*; Sep. 1990

NIFS-53 M.Okamoto and N.Nakajima, *Bootstrap Currents in Stellarators and Tokamaks*; Sep. 1990

NIFS-54 K.Itoh and S.-I.Itoh, *Peaked-Density Profile Mode and Improved Confinement in Helical Systems*; Oct. 1990

NIFS-55 Y.Ueda, T.Enomoto and H.B.Stewart, *Chaotic Transients and Fractal Structures Governing Coupled Swing Dynamics*; Oct. 1990

NIFS-56 H.B.Stewart and Y.Ueda, *Catastrophes with Indeterminate Outcome*; Oct. 1990

NIFS-57 S.-I.Itoh, H.Maeda and Y.Miura, *Improved Modes and the Evaluation of Confinement Improvement*; Oct. 1990

NIFS-58 H.Maeda and S.-I.Itoh, *The Significance of Medium- or Small-size Devices in Fusion Research*; Oct. 1990

NIFS-59 A.Fukuyama, S.-I.Itoh, K.Itoh, K.Hamamatsu, V.S.Chan, S.C.Chiu, R.L.Miller and T.Ohkawa, *Nonresonant Current Drive by RF Helicity Injection*; Oct. 1990

NIFS-60 K.Ida, H.Yamada, H.Iguchi, S.Hidekuma, H.Sanuki, K.Yamazaki and CHS Group, *Electric Field Profile of CHS Heliotron/Torsatron Plasma with Tangential Neutral Beam Injection*; Oct. 1990

NIFS-61 T.Yabe and H.Hoshino, *Two- and Three-Dimensional Behavior of Rayleigh-Taylor and Kelvin-Helmholz Instabilities*; Oct. 1990

NIFS-62 H.B. Stewart, *Application of Fixed Point Theory to Chaotic Attractors of Forced Oscillators;* Nov. 1990

NIFS-63 K.Konn., M.Mituhashi, Yoshi H.Ichikawa,*Soliton on Thin Vortex Filament;* Dec. 1990

NIFS-64 K.Itoh, S.-I.Itoh and A.Fukuyama,*Impact of Improved Confinement on Fusion Research;* Dec. 1990

NIFS -65 A.Fukuyama, S.-I.Itoh and K. Itoh,*A Consistency Analysis on the Tokamak Reactor Plasmas;* Dec. 1990

NIFS-66 K.Itoh, H. Sanuki, S.-I. Itoh and K. Tani,*Effect of Radial Electric Field on α-Particle Loss in Tokamaks;* Dec. 1990

NIFS-67 K.Sato,and F.Miyawaki,*Effects of a Nonuniform Open Magnetic Field on the Plasma Presheath*; Jan.1991

NIFS-68 K.Itoh and S.-I.Itoh,*On Relation between Local Transport Coefficient and Global Confinement Scaling Law;* Jan. 1991

NIFS-69 T.Kato, K.Masai, T.Fujimoto,F.Koike, E.Källne, E.S.Marmar and J.E.Rice,*He-like Spectra Through Charge Exchange Processes in Tokamak Plasmas;* Jan.1991

NIFS-70 K. Ida, H. Yamada, H. Iguchi, K. Itoh and CHS Group, *Observation of Parallel Viscosity in the CHS Heliotron/Torsatron* ; Jan.1991

NIFS-71 H. Kaneko, *Spectral Analysis of the Heliotron Field with the Toroidal Harmonic Function in a Study of the Structure of Built-in Divertor* ; Jan. 1991

NIFS-72 S. -I. Itoh, H. Sanuki and K. Itoh, *Effect of Electric Field Inhomogeneities on Drift Wave Instabilities and Anomalous Transport* ; Jan. 1991

NIFS-73 Y.Nomura, Yoshi.H.Ichikawa and W.Horton, *Stabilities of Regular Motion in the Relativistic Standard Map*; Feb. 1991

NIFS-74 T.Yamagishi, *Electrostatic Drift Mode in Toroidal Plasma with Minority Energetic Particles,* Feb. 1991

NIFS-75 T.Yamagishi, *Effect of Energetic Particle Distribution on Bounce Resonance Excitation of the Ideal Ballooning Mode,* Feb. 1991

NIFS-76 T.Hayashi, A.Tadei, N.Ohyabu and T.Sato, *Suppression of Magnetic Surface Breading by Simple Extra Coils in Finite Beta Equilibrium of Helical System;* Feb. 1991

NIFS-77 N. Ohyabu, *High Temperature Divertor Plasma Operation*; Feb. 1991

NIFS-78 K.Kusano, T. Tamano and T. Sato, *Simulation Study of Toroidal Phase-Locking Mechanism in Reversed-Field Pinch Plasma*; Feb. 1991

NIFS-79 K. Nagasaki, K. Itoh and S. -I. Itoh, *Model of Divertor Biasing and Control of Scrape-off Layer and Divertor Plasmas*; Feb. 1991

NIFS-80 K. Nagasaki and K. Itoh, *Decay Process of a Magnetic Island by Forced Reconnection*; Mar. 1991

NIFS-81 K. Takahata, N. Yanagi, T. Mito, J. Yamamoto, O.Motojima and LHDDesign Group, K. Nakamoto, S. Mizukami, K. Kitamura, Y. Wachi, H. Shinohara, K. Yamamoto, M. Shibui, T. Uchida and K. Nakayama, *Design and Fabrication of Forced-Flow Coils as R&D Program for Large Helical Device*; Mar. 1991

NIFS-82 T. Aoki and T. Yabe, *Multi-dimensional Cubic Interpolation for ICF Hydrodynamics Simulation*; Apr. 1991

NIFS-83 K. Ida, S.-I. Itoh, K. Itoh, S. Hidekuma, Y. Miura, H. Kawashima, M. Mori, T. Matsuda, N. Suzuki, H. Tamai, T.Yamauchi and JFT-2M Group, *Density Peaking in the JFT-2M Tokamak Plasma with Counter Neutral Beam Injection* ; May 1991

NIFS-84 A. Iiyoshi, *Development of the Stellarator/Heliotron Research*; May 1991

NIFS-85 Y. Okabe, M. Sasao, H. Yamaoka, M. Wada and J. Fujita, *Dependence of Au^- Production upon the Target Work Function in a Plasma-Sputter-Type Negative Ion Source;* May 1991

NIFS-86 N. Nakajima and M. Okamoto, *Geometrical Effects of the Magnetic Field on the Neoclassical Flow, Current and Rotation in General Toroidal Systems*; May 1991

NIFS-87 S. -I. Itoh, K. Itoh, A. Fukuyama, Y. Miura and JFT-2M Group, *ELMy-H mode as Limit Cycle and Chaotic Oscillations in Tokamak Plasmas;* May 1991

NIFS-88 N.Matsunami and K.Kitoh, *High Resolution Spectroscopy of H^+ Energy Loss in Thin Carbon Film;* May 1991

NIFS-89 H. Sugama, N. Nakajima and M.Wakatani, *Nonlinear Behavior of Multiple-Helicity Resistive Interchange Modes near Marginally Stable States;* May 1991

NIFS-90 H. Hojo and T.Hatori, *Radial Transport Induced by Rotating RF Fields and Breakdown of Intrinsic Ambipolarity in a Magnetic Mirror*; Jun. 1991

NIFS-91 M. Tanaka, S. Murakami, H. Takamaru and T.Sato, *Macroscale Implicit, Electromagnetic Particle Simulation of Inhomogeneous and Magnetized Plasmas in Multi-Dimensions;* Jun. 1991

NIFS-92 S. - I. Itoh, *H-mode Physics, -Experimental Observations and Model Theories-, Lecture Notes, Spring College on Plasma Physics, May 27 - June 21 1991 at International Centre for Theoretical Physics (IAEA UNESCO) Trieste, Italy ;* Jun. 1991

NIFS-93 Y. Miura, K. Itoh, S. - I. Itoh, T. Takizuka, H. Tamai, T. Matsuda, N. Suzuki, M. Mori, H. Maeda and O. Kardaun, *Geometric Dependence of the Scaling Law on the Energy Confinement Time in H-mode Discharges;* Jun. 1991

NIFS-94 H. Sanuki, K. Itoh, K. Ida and S. - I. Itoh, *On Radial Electric Field Structure in CHS Torsatron / Heliotron;* Jun. 1991

NIFS-95 K. Itoh, H. Sanuki and S. - I. Itoh, *Influence of Fast Ion Loss on Radial Electric Field in Wendelstein VII-A Stellarator;* Jun. 1991

NIFS-96 S. - I. Itoh, K. Itoh, A. Fukuyama, *ELMy-H mode as Limit Cycle and Chaotic Oscillations in Tokamak Plasmas;* Jun. 1991

NIFS-97 K. Itoh, S. - I. Itoh, H. Sanuki, A. Fukuyama, *An H-mode-Like Bifurcation in Core Plasma of Stellarators;* Jun. 1991

NIFS-98 H. Hojo, T. Watanabe, M. Inutake, M. Ichimura and S. Miyoshi, *Axial Pressure Profile Effects on Flute Interchange Stability in the Tandem Mirror GAMMA 10;* Jun. 1991

NIFS-99 A. Usadi, A. Kageyama, K. Watanabe and T. Sato, *A Global Simulation of the Magnetosphere with a Long Tail : Southward and Northward IMF;* Jun. 1991

NIFS-100 H. Hojo, T. Ogawa and M. Kono, *Fluid Description of Ponderomotive Force Compatible with the Kinetic One in a Warm Plasma* ; July 1991

NIFS-101 H. Momota, A. Ishida, Y. Kohzaki, G. H. Miley, S. Ohi, M. Ohnishi K. Yoshikawa, K. Sato, L. C. Steinhauer, Y. Tomita and M. Tuszewski *Conceptual Design of D-^{3}He FRC Reactor "ARTEMIS"* ; July 1991

NIFS-102 N. Nakajima and M. Okamoto, *Rotations of Bulk Ions and Impurities in Non-Axisymmetric Toroidal Systems* ; July 1991